AGU PUBLICATIONS

Tectonics

RESEARCH ARTICLE
10.1002/2017TC004617

Key Points:
- We address the relationships between the lower crustal *T*-Reflection and the high-velocity and high-density Lower Crustal Body (LCB) on the Vøring Margin using integrated multidisciplinary geophysical data sets
- The *T*-Reflection represents a high impedance boundary associated with intruded sills with different shapes and characters
- The LCB is made of a mixture of pre- and syn-breakup mafic and ultramafic rocks associated with older metamorphic rocks such as granulites and eclogites

Correspondence to:
M. M. Abdelmalak,
m.m.abdelmalak@geo.uio.no;
abdelmalak@vbpr.no;
abdelmalak_mansour@yahoo.fr

Citation:
Abdelmalak, M. M., Faleide, J. I., Planke, S., Gernigon, L., Zastrozhnov, D., Shephard, G. E., & Myklebust, R. (2017). The *T*-Reflection and the deep crustal structure of the Vøring Margin, offshore mid-Norway. *Tectonics*, *36*, 2497–2523. https://doi.org/10.1002/2017TC004617

Received 12 APR 2017
Accepted 7 OCT 2017
Accepted article online 17 OCT 2017
Published online 14 NOV 2017

The *T*-Reflection and the Deep Crustal Structure of the Vøring Margin, Offshore mid-Norway

M. M. Abdelmalak[1,2], J. I. Faleide[1], S. Planke[1,2], L. Gernigon[3], D. Zastrozhnov[1,2], G. E. Shephard[1], and R. Myklebust[4]

[1]Centre for Earth Evolution and Dynamics (CEED), University of Oslo, Oslo, Norway, [2]Volcanic Basin Petroleum Research (VBPR), Oslo Science Park, Oslo, Norway, [3]Geological Survey of Norway (NGU), Trondheim, Norway, [4]TGS, Asker, Norway

Abstract Seismic reflection data along volcanic passive margins frequently provide imaging of strong and laterally continuous reflections in the middle and lower crust. We have completed a detailed 2-D seismic interpretation of the deep crustal structure of the Vøring Margin, offshore mid-Norway, where high-quality seismic data allow the identification of high-amplitude reflections, locally referred to as the *T*-Reflection. Using a dense seismic grid, we have mapped the geometry of the *T*-Reflection in order to compare it with filtered Bouguer gravity anomalies and seismic refraction data. The *T*-Reflection is identified between 7 and 10 s. Sometimes it consists of one single smooth reflection. However, it is frequently associated with a set of rough multiple reflections displaying discontinuous segments with varying geometries, amplitudes, and contact relationships. The *T*-Reflection seems to be connected to deep sill networks and is locally identified at the continuation of basement high structures or terminates over fractures and faults. The *T*-Reflection presents a low magnetic signal. The spatial correlation between the filtered positive Bouguer gravity anomalies and the deep dome-shaped reflections indicates that the latter represent a high-impedance boundary contrast associated with a high-density and high-velocity body. In ~50% of the outer Vøring Margin, the depth of the mapped *T*-Reflection is found to correspond to the depth of the top of the Lower Crustal Body (LCB), which is characterized by high *P* wave velocities (>7 km/s). We present a tectonic scenario, where a large part of the deep crustal structure is composed of preserved upper continental crustal blocks and middle to lower crustal lenses of inherited high-grade metamorphic rocks. Deep intrusions into the faulted crustal blocks are responsible for the rough character of the *T*-Reflection, whereas intrusions into the ductile lower crust and detachment faults are likely responsible for its smoother character. Deep magma intrusions can be responsible for regional metamorphic processes leading to an increasing velocity of the lower crust to more than 7 km/s. The result is a heterogeneous LCB that likely represents a complex mixture of pre- to syn-breakup mafic and ultramafic rocks (cumulates and sills) and old metamorphic rocks such as granulites and eclogites. An increasing degree of melting toward the breakup axis is responsible for an increasing proportion of cumulates and sill intrusions in the lower crust.

1. Introduction

The increased availability of high-quality seismic and potential field data, combined with deep sea drilling and onshore analogue studies, has shown that extensional processes can lead to complex crustal configurations, depending on lithospheric composition, thermal structure and heat transfer, far field stresses, extension rate and duration, mantle flow, and structural inheritance (Clerc et al., 2017; England, 1983; Koptev et al., 2015; Kusznir & Park, 1987; Lavecchia et al., 2017; Reston, 2007; Rosenbaum et al., 2008; Ziegler & Cloetingh, 2004). Many studies have led to a range of conceptual and numerical models of plate breakup at magma-poor margins (Brune et al., 2017; Huismans & Beaumont, 2003; Lavier & Manatschal, 2006; Pérez-Gussinyé, 2012). However, more than 50% of passive margins worldwide are interpreted to be magma-rich (Coffin & Eldholm, 1994; Menzies et al., 2002; Skogseid, 2001). These are characterized by massive occurrence of mafic extrusive and intrusive rocks, emplaced before and during plate breakup (e.g., Abdelmalak, 2010; Abdelmalak et al., 2012; Eldholm & Grue, 1994; Geoffroy, 2005), and playing a major role in determining the evolution and the deep structure of magma-rich margins. Seismic reflection data along volcanic passive margins frequently provide imaging of strong and laterally continuous crustal reflections in the middle and lower crusts (e.g., Clerc et al., 2015; Kusznir et al., 2015).

In the NE Atlantic (Figure 1A), wide-angle seismic surveying across most of the conjugate volcanic margins revealed high-velocity layers at the base of the crust referred to as Lower Crustal Bodies (LCBs; Holbrook

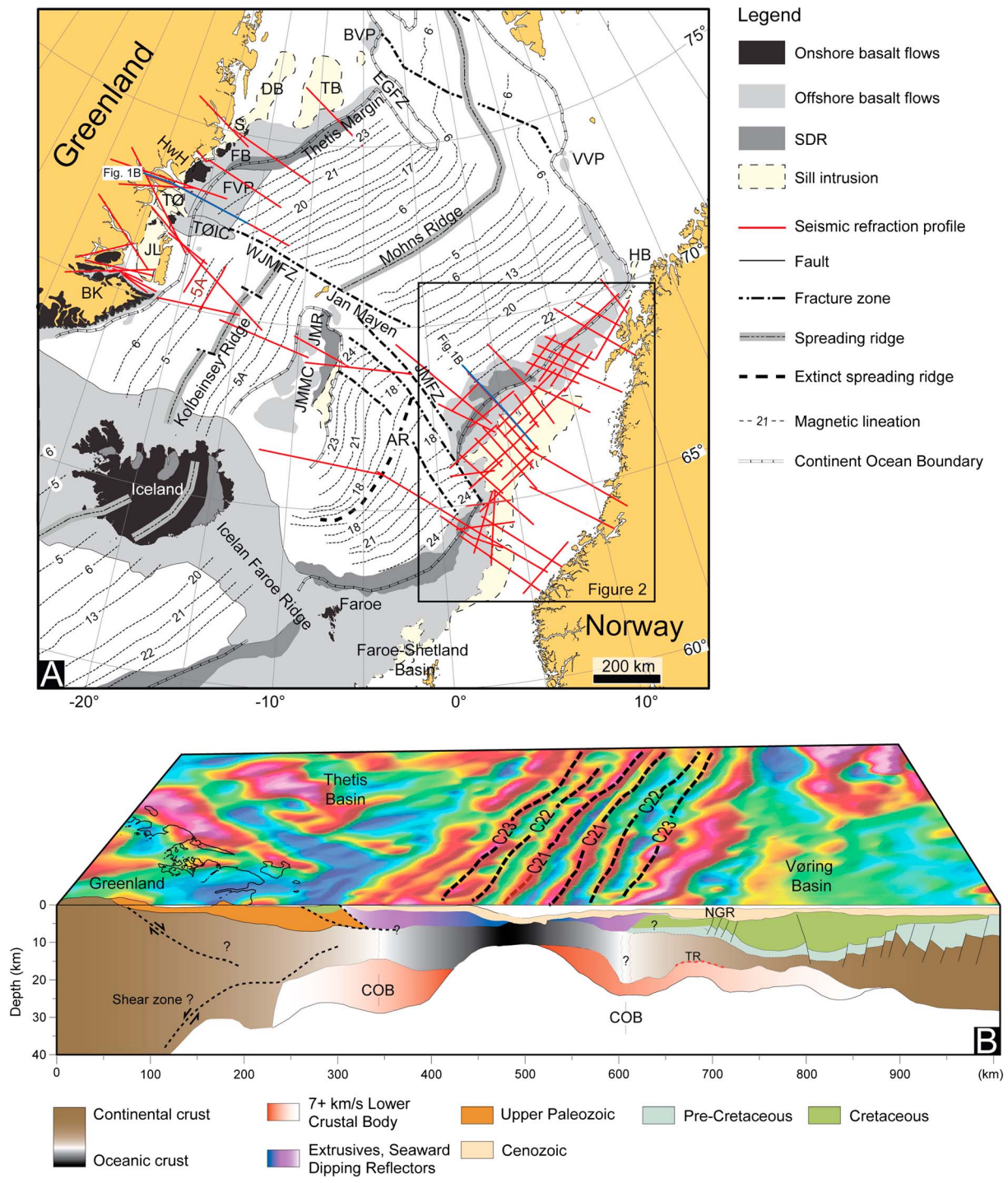

Figure 1. (A) Onshore and offshore distribution of the basalt flows in the North Atlantic Igneous Province (Abdelmalak et al., 2014). The Seaward Dipping Reflectors (SDR) locations and different refraction profiles used in this study are indicated (see the text for data references). (B) 3-D reconstruction at C21 (~47 Ma) of the crustal structure across the Vøring Margin (Faleide et al., 2008) and its conjugate Greenland margin in the Thetis Basin (Schlindwein & Jokat, 1999; Voss & Jokat, 2007). The magnetic anomalies are defined using released magnetic data EMAG2 (Maus et al., 2009). The continent–ocean boundary (COB) is indicated for the conjugate margins. Dashed black lines indicate shear zones. NGR: North Gjallar Ridge; TR: *T*-Reflection (dashed red line). AR: Aegir Ridge; BK: Blosseville Kyst; BVP: Boreas Volcanic Province; DB: Danmarkshavn Basin; EGFZ: East Greenland Fault Zone; FB: Foster Basin; FVP: Foster Volcanic Province; HB: Harstad Basin; HwH: Hold with Hope; JL: Jamson Land; JMFZ: Jan Mayen Fracture Zone; JMMC: Jan Mayen Micro-Continent; JMR: Jan Mayen Ridge; S: Shannon; TB: Thetis Basin; TØ: Traill Ø; TØIC: Traill Ø Igneous Complex; VVP: Vestbakken Volcanic Province; WJMFZ: West Jan Mayen Fracture Zone.

et al., 2001; Klingelhöfer et al., 2005; Mjelde et al., 2007; Mjelde, Raum, et al., 2009; Mjelde, Raum, Myhren, et al., 2005; Roberts et al., 2009; Schiffer et al., 2016; Voss & Jokat, 2007; Voss et al., 2009; Figure 1B). LCBs are characterized by *P* wave velocities (V_p) of 7.1 to 7.7 km/s and V_p/V_s ratios ranging between 1.8 and 1.9 (Mjelde, Raum, et al., 2003; O'Reilly et al., 1996). The nature and origin of the LCBs are still controversial and probably more complex than hitherto thought (e.g., Ebbing et al., 2006; Gernigon et al., 2004; Mjelde et al., 2016). Early studies have proposed that the anomalously high velocities in the LCBs represent massive mafic magmatic underplating emplaced during the final stage of rifting and continental breakup. In this context, LCBs could be explained by magma showing high concentrations of MgO, which in turn may reflect high asthenospheric temperatures and/or compositional inhomogeneities in the asthenospheric source (e.g., R. S. White & McKenzie, 1989).

Lower Crustal Bodies are often located along the continent–ocean transition (COT; Eldholm et al., 2000) but can extend continentward, outside the identified volcanic province (Kvarven et al., 2014; Mjelde et al., 2016; Nirrengarten et al., 2014). In recent years, discussion about the interpretation of the LCBs focuses on its nature in terms of magmatic versus inherited and/or serpentinized material (Ebbing et al., 2006; Fichler et al., 2011; Lundin & Doré, 2011; Mjelde et al., 2002; Reynisson et al., 2010; Wangen et al., 2011). Given the strong overlap of the geophysical values attributed to continental crust, as well as mafic and ultramafic rocks, the geophysical modeling of LCBs alone does not easily permit the preference of one interpretation over the other, but rather, the observed correlation with structure allows the discussion of scenarios and realistic hypotheses (Gernigon et al., 2004; Ren et al., 1998; Schiffer et al., 2016). In such conditions, the architecture of rifted margins is still the subject of debate in order to explain its structural, stratigraphic, and magmatic evolution.

On the other hand, the interactions between magmatism, deep structures, and extensional processes are also not completely understood. Generally, transport of mafic magma through the upper brittle crust is widely viewed as being dominated by dykes (Lister & Kerr, 1991; Rubin, 1995), which are often invoked as the main feeders for flood basalt sequences (Abdelmalak et al., 2015; Coffin & Eldholm, 1994; Ernst et al., 1995; Klausen & Larsen, 2002). In contrast to dykes, bedding-parallel sills are widely regarded as having only a limited role in vertical magma transport. How deep sill complexes along volcanic margin are associated with LCBs, or not, is a challenging problem. To address these issues, it is common to supplement the reflection-based seismic interpretation with velocity and density models derived from refraction and potential field studies (e.g., Corseri et al., 2017).

High-amplitude deep crustal reflections, located at depths >6–7 s, have been imaged in the outer Vøring Basin. Reflections display a domal shape below the South and North Gjallar ridges and have been interpreted as the top of a core complex of melted crust triggered by underplating and labelled "mid-crustal convex-up reflector" (Lundin & Doré, 1997) or "MCD" for "middle crustal dome" (Ren et al., 1998) in the North Gjallar Ridge. In later studies, these reflections have been regionally mapped along the outer Vøring Basin and named the *T*-Reflection (Gernigon et al., 2001). In the North and South Gjallar ridges, Gernigon et al. (2003) further discussed the definition and structural interpretation of the *T*-Reflection and suggested that it coincides with the top of the continental part of the LCB geophysically modeled at approximately the same depth based on ocean bottom seismometer (OBS) data (Mjelde, Faleide, et al., 2009; Rouzo et al., 2006; Figure 1). The part of the LCB imaged beneath the North Gjallar Ridge appears to have been emplaced before the main volcanic event and influenced the faulting and distal development of the sedimentary basin at least 10–15 Ma before the breakup and the main magmatic event (Gernigon et al., 2004).

The aim of this study was to determine the nature and origin of the deep crust along the conjugate volcanic margins of the Norwegian–Greenland Sea. Despite expansive coverage of seismic data along the mid-Norwegian Margin (Figure 3B), several questions about the deep structure of rifted margins remain unresolved: (1) What is the origin of the *T*-Reflection? (2) What are the relationships between the *T*-Reflection, basin deformation, continental breakup, and the LCB? (3) What is the origin of the LCB in the continental and distal parts of the rifted margin? (4) Are LCBs fully representative of breakup-related igneous rocks? To answer these questions, we have investigated the structure, nature, and possible origins of the *T*-Reflection based on the use of new and combined geophysical data sets (reflection and refraction seismic, gravity, and magnetic data).

2. Geological Setting

The conjugate volcanic rifted margins along the Norwegian–Greenland Sea are parts of the North Atlantic large igneous province formed during the continental breakup in the Paleogene (Eldholm et al., 2000;

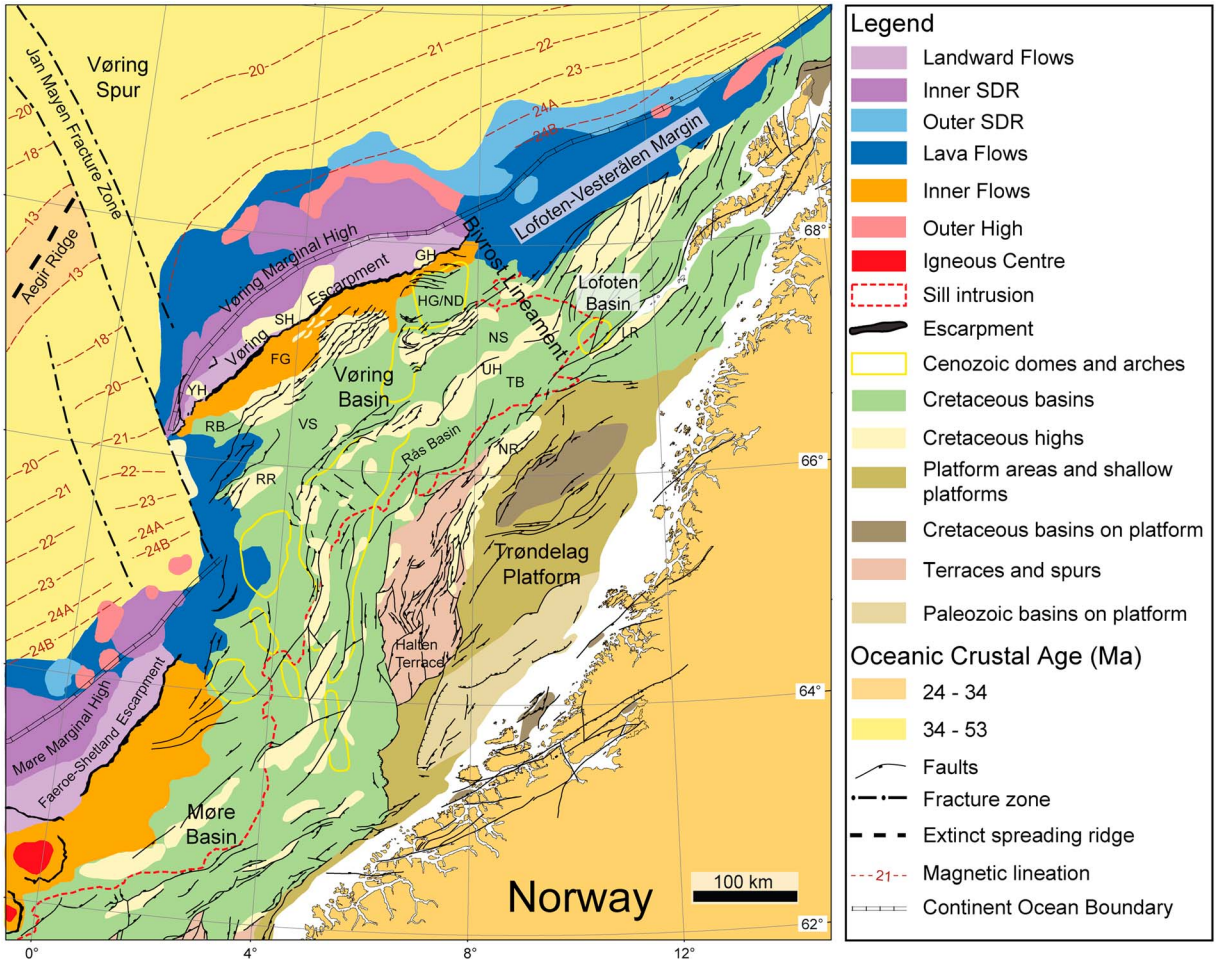

Figure 2. Simplified map of the mid-Norwegian margin showing the main tectonic units, fault zones (using our new seismic interpretation and modified from Blystad et al., 1995; and Gernigon et al., 2003), and volcanic seismic facies units (using our new seismic interpretation and modified from Berndt et al., 2001). FG: Fenris Graben; GH: Grimm High; HG/ND: Hel Graben/Nagfar Dome; NR: Norland Ridge; NS: Någrind Syncline; RB: Rån Basin; RR: Rån Ridge; SDRs: Seward dipping reflectors; SH: Skoll High; TB: Træna Basin; UH: Utgard High; VS: Vigrid Syncline; YH: Ygg High.

Meyer et al., 2007; Saunders et al., 1997; Figure 1). The onset of continental breakup marked the culmination of a ~300 Ma period of extension and basin formation subsequent to the Caledonian orogeny (Doré et al., 1999; Skogseid et al., 2000; Tsikalas et al., 2008; Ziegler, 1988). The main extensional events occurred in Late Paleozoic–Triassic, Late Jurassic–Early/Middle Cretaceous, and Late Cretaceous–Paleocene times (Brekke, 2000; Eldholm & Grue, 1994; Gernigon et al., 2004; Lundin & Doré, 2005). Through the Paleozoic and Mesozoic, lithospheric thinning resulted in the formation of large sedimentary basins controlled by normal faults (e.g., Faleide et al., 2008; Tsikalas et al., 2012). Subsidence was especially important during the Cretaceous, giving rise to the accumulation of up to 8 km of sediments in local depocenters in the Vøring and Møre basins (Blystad et al., 1995; Brekke, 2000; Lien, 2005; Scheck-Wenderoth et al., 2007).

On the Vøring Margin, the Late Jurassic–Early/mid-Cretaceous extension and the Late Cretaceous extension formed large-scale rift blocks and structural highs (Early Cretaceous ridges and highs: Rån Ridge, Utgard High; Late Cretaceous–Early Paleocene ridges and highs: North and South Gjallar ridges, Nyk High, Ygg High, Grimm High, and Skoll High) separated by subbasins such as the Træna Basin, the Någrind Syncline, the Rån Basin, the Rås Basin, the Vigrid Syncline, and the Fenris Graben (Abdelmalak, Planke, et al., 2016; Figure 2). During the Late Cretaceous–Paleocene, the locus of maximum extension migrated NW toward the zone of the future continental separation (Skogseid et al., 2000). The final continental breakup recorded in the Vøring Marginal High occurred at early Eocene (~56–55 Ma according to Gradstein et al., 2012, time-scale) and resulted in voluminous extrusive and intrusive igneous activities within the adjacent

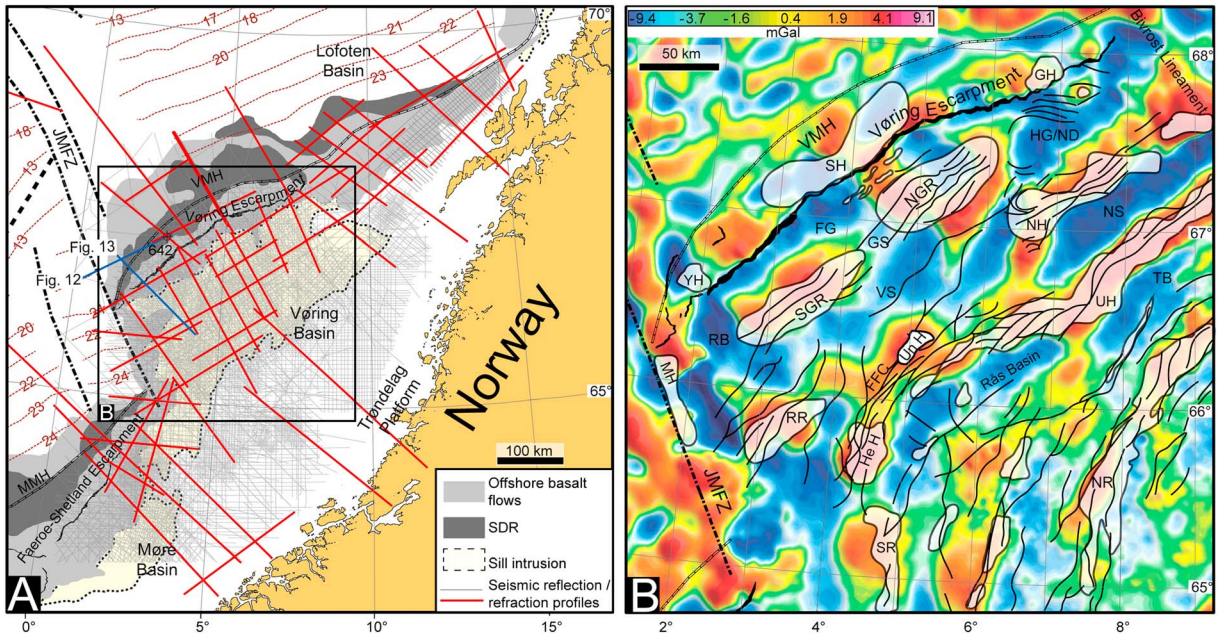

Figure 3. (A) Seismic reflection data used in this study. (B) Bouguer residual gravity anomaly, 50 km high-pass filtered. White shaded areas correspond to structural highs. Black lines indicate faults. Gravity data courtesy of TGS. FFC: Fles Fault Complex; FG: Fenris Graben; GH: Grimm High; GS: Gleipne Saddle; HeH: Hevring High; HG/ND: Hel Graben/Nagfar Dome; NH: Nyk High; NGR: North Gjallar Ridge; NR: Norland Ridge; NS: Någrind Syncline; MH: Mimir High; MMH: Møre Marginal High; RB: Rån Basin; RR: Rån Ridge; SGR: South Gjallar Ridge; SH: Skoll High; SR: Slettringen Ridge; TB: Træna Basin; UH: Utgard High; UnH: Unn High; VMH: Vøring Marginal High; VS: Vigrid Syncline; YH: Ygg High.

sedimentary basins and preexisting continental crust (Breivik et al., 2014; Eldholm & Grue, 1994; Hinz, 1981; Mjelde et al., 2007; Mutter et al., 1982; Planke et al., 2005; R. S. White & McKenzie, 1989; Figure 2).

On the NE Greenland side, extrusive volcanism is also exposed in several places onshore (e.g., Brooks, 2011; Geissler et al., 2016; Larsen et al., 2014; Tegner et al., 1998; e.g., Shannon Island, Blosseville Kyst area, Hold with Hope; Figure 1A). Offshore, a thin volcanic complex, extending approximately 110 km, is mapped along the Thetis Margin. Seaward Dipping Reflectors (SDRs) are observed east of this volcanic complex where they are located approximately along the continent–ocean boundary (Abdelmalak, Planke, et al., 2016). The SDRs pinch out to the south against the Foster Volcanic Province, which is bounded by the Traill Ø Igneous Complex to the south and the Foster Basin to the north (Figure 1A). The Foster Volcanic Province consists of thick volcanic flows draped by Eocene and younger sediments (Reynolds et al., 2017). However, it has been classified as transitional crust by Voss and Jokat (2007). Nonetheless, we consider the Foster Volcanic Province as an oceanic plateau. Further south, the Traill Ø Igneous Complex defines a trend parallel to the West Jan Mayen Fracture Zone. The formation of this igneous complex is linked to the breakup between East Greenland and the Jan Mayen Micro-Continent during the Late Eocene–Oligocene time. North of the East Greenland Fracture Zone, the Boreas Volcanic Province is considered to be the conjugate to the Vestbakken Volcanic Province in the SW Barents Sea (Figure 1A).

3. Data and Methods

3.1. Data

This work is based on the interpretation of a dense grid of more than 1,200 regional 2-D seismic lines with a total length of more than 150,000 km and with a spacing ranging between 0.2 and 2 km (Figure 3A). This data set includes recently acquired as well as reprocessed high-quality seismic reflection data that provide improved imaging of the deeper parts of the margin. The new data include, notably, 10,000 km of the MNR-11 seismic survey acquired in 2011 by TGS and Fugro. Our database also comprises previous long-offset seismic surveys including in particular the VMT-95, VBT-94, and the GMNR-94 surveys, which were recorded with 11 to 14 s (two-way travel time).

In addition, more than 40 refraction profiles from the Møre, Vøring, and Lofoten-Vesterålen margins have been used in this study (e.g., Breivik et al., 2009, 2014; Mjelde et al., 1996, 2007; Mjelde, Raum, et al., 2009; Mjelde, Raum, Breivik, et al., 2005; Raum et al., 2002, 2006; Figure 3A). Conjugate refraction profiles from NE Greenland (e.g., Hermann, 2013; Schlindwein & Jokat, 1999; Schmidt-Aursch & Jokat, 2005; Voss & Jokat, 2007; Voss et al., 2009; Weigel et al., 1995) and Jan Mayen (e.g., Breivik et al., 2012) margins have also been considered (Figure 1A). These data have been used to compare the different velocity models of the crust and the difference between the reflection and refraction seismic data.

Ship-borne gravity and magnetic data have been acquired along most of the seismic profiles of the mid-Norwegian margin. The data have been processed and gridded by TGS. The data have been combined with regional public grids of satellite gravity (Sandwell & Smith, 2009), magnetic compilations (Maus et al., 2009; Verhoef et al., 1996), and bathymetry (GEBCO centenary edition). The gravity data have been Bouguer corrected using a correction density of 2,200 kg/m^3. Both the gravity and magnetic grids have been high-pass filtered with cutoff wavelengths of 50, 100, 200, and 400 km.

3.2. Methods

The regional seismic interpretation was carried out using the SMT Kingdom Suite software (www.ihs.com). We mapped the *T*-Reflection horizon in the outer Vøring Margin based on its strong amplitude characteristics. The seismic line density was high enough to laterally correlate the deep crustal reflections and to generate grids.

Bouguer-corrected gravity maps are useful for geological interpretations as the effect of water depth variations is mainly removed (e.g., Berndt, 2002). The Bouguer anomaly map mainly reflects variations in crustal thickness. A high-pass filtered Bouguer anomaly map with a cutoff wavelength of 50 km emphasizes the deep basin and midcrustal density variations, with typical source depths of less than 10 km. The anomaly pattern (e.g., wavelength and amplitude) provides information about fault blocks and configuration of subbasins (e.g., Berndt, 2002; Figure 3B). Magnetic anomaly maps may reveal large tectonic trends and define oceanic crust with characteristic sea floor spreading anomalies. High-pass filtered magnetic anomaly maps usually highlight middle and upper crustal variations. The wavelength and amplitude of anomalies provide information about depth to source and magnetic properties. The high-amplitude positive magnetic anomalies on the shelf often correspond to basement ridges or shallow igneous rocks, whereas negative anomalies are generally associated with deep sedimentary strata. High-pass filtered potential field data were scaled to two-way travel time, converted to pseudohorizons, and loaded into the workstation to facilitate the joint interpretation of seismic and potential field data (e.g., Planke et al., 2015).

To improve the 2-D deep crustal interpretation, several key refraction profiles were time-converted (to two-way travel time) and loaded into the workstation. This approach allowed us to display the crustal and the velocity structure along the seismic reflection data for comparison. The grid generated from seismic horizon picking (the *T*-Reflection grid) was depth converted with HiQbe^{TM} (http://www.first-geo.com/products/hiqbe/norway), a regional seismic velocity cube covering the mid-Norwegian margin and compiled from 536 seismic stacking velocity data sets and 230 check shots from wells and vertical seismic profile data. The stacking velocities used for the depth conversion are constraining the velocity structure of the sedimentary basin where reflections are imaged. At greater depths, a delta-anisotropy function was used for depth conversion (e.g., Thomsen, 1986). The stacking velocities are, however, lower than the OBS velocities because of differences in the frequency content and the paths of wave propagation (Thomsen, 1986). The HiQbe^{TM} velocity cube intends to replicate the velocity for true vertical wave propagation, while OBS data are modeled with a great horizontal component often without taking into concern the anisotropic effect (horizontal being greater than vertical velocity, in general). Consequently, the HiQbe^{TM} is presented with average velocities (from sea surface down to target depth), while OBS data are mostly presented as interval velocities (layer-specific velocities) where interval velocities are often higher (~10–15%) than the average velocities. Combined with uncertainties related to the different modeling techniques, additional errors could be driven by uncertainties in the OBS velocity forward modeling. These considerations will lead to obvious uncertainties and differences when comparing refraction and depth-converted reflection data. However, by comparing the stacking velocities and OBS velocity in selected 1-D profiles in the Vøring Margin, we found comparable results in most of the cases.

4. Results

4.1. The Vøring Margin Structure

The 50 km high-pass filtered Bouguer gravity anomaly map reveals a complex pattern of positive and negative amplitude anomalies along the Vøring Margin (Figure 3B). In the Vøring Basin, several elongated negative gravity anomalies, striking NE–SW, are identified and correspond to the Hel Graben, Fenris Graben, Vigrid Syncline, Någrind Syncline, Træna Basin, and Rås Basin. These different subbasins are separated by NE-SW elongated positive anomalies, corresponding to the Nyk High, the North and South Gjallar ridges, and the Utgard High. The Rån Ridge approximately coincides with an ENE–WSW positive anomaly. High-amplitude rounded positive gravity anomalies are distributed along the Vøring Escarpment and correspond to positive elongated NE-trending magnetic anomalies (Abdelmalak, Planke, et al., 2016; Planke et al., 2017). Oceanward of the Vøring Escarpment, the gravity anomalies likely represent intra- and subbasalt structural highs. These anomalies correspond to Skoll High, Grimm High, and Ygg High, as also observed on seismic data. Toward the SW Vøring Basin, the gravity anomalies change orientation from NE–SE (Unn High) to approximately N–S (Slettringen Ridge; Figure 3B).

4.2. Reflection Data: The *T*-Reflection

From reprocessed and high-quality seismic data in the Vøring Margin, a more accurate interpretation from the shallow parts to the deeper parts of the margin, down to the *T*-Reflection, is now possible. Examples of the reprocessed seismic data, shown in Figure 4, illustrate the main elements discussed in this paper. For the shallow parts, the base Tertiary unconformity represents a regional erosional surface onlapped by Paleogene sediments. The base Cretaceous unconformity (BCU) is robustly mapped landward of the basalt. The BCU is generally considered to record the rift climax activity of the major Late Jurassic–Early Cretaceous extensional phase and is often used as a key regional marker to constrain the spatial and temporal history of the Late Jurassic-Early Cretaceous rift system (Blystad et al., 1995). Below the basalt, the seismic imaging is of poor quality but confirms locally that volcanic basins do exist underneath the lava flows. The BCU is deeper below the Rån Basin and the Vigrid Syncline and shallows below the South Gjallar and Rån ridges. Several low-angle faults characterizing the Cretaceous and the pre-Cretaceous sediments are assumed to be of at least Early Campanian–Early Paleocene age (Gernigon et al., 2003; Ren et al., 2003). Jurassic to Early/middle Cretaceous faulting was previously observed on the Rån Ridge area where the BCU and older syn-rift sequences could be clearly identified near the basalts (Gernigon et al., 2001, 2003). Abundant Paleogene sill intrusions are also identified within the Cretaceous and pre-Cretaceous sequences.

For the deeper part, the outer Vøring Basin displays a well-defined high-amplitude and strong reflection with variable continuity and coherence referred to as the *T*-Reflection (Gernigon et al., 2003, 2004). This high-amplitude deep crustal reflection is observed at depths ranging between 7 and 10 s (Figures 4 and 5). In the seismic data, the *T*-Reflection is sometimes smooth and is primarily identified on a single event (Figures 5A and 5B). Sometimes the *T*-Reflection is associated with a series of reflections (Figure 5D). It is therefore discontinuous and displays distinct steep and flat segments with varying geometries, amplitude, and contact relationships (Figures 5C and 5D).

In this paper we discuss the *T*-Reflection as a single characteristic feature, regardless of its shape and number of cycles. Our seismic interpretation reveals that the *T*-Reflection is mainly identified in the outer Vøring Basin and extends between the Vøring Escarpment and Fles Fault Complex and Utgard High (Figure 6A). West of the Vøring Escarpment, the *T*-Reflection is difficult to map beneath the thick volcanic extrusives that give rise to scattering of the seismic energy. The *T*-Reflection is clearly mapped in the North Gjallar Ridge where the high-amplitude reflection is rather continuous, shows a smooth shape, and can be mapped laterally over 50 km (Figure 6B). In the southwest Vøring Basin, the *T*-Reflection can be identified over more than 150 km along the Rån Basin, Rån Ridge, and Vigrid Syncline (Figure 6B).

Beneath the northwestern parts of the North Gjallar, South Gjallar, and Rån ridges, the *T*-Reflection exhibits domal shapes of more than 20 km in diameter, with its shallowest part between 7 and 8 s. Compared to the first map of the *T*-Reflection (Gernigon et al., 2003), our new and denser seismic data set permits the identification of additional subtle variations across the Rån and the South Gjallar ridges. Less prominent *T*-Reflection domes (Figure 6A) are now observed below the so-called Hevring High, Unn High, and

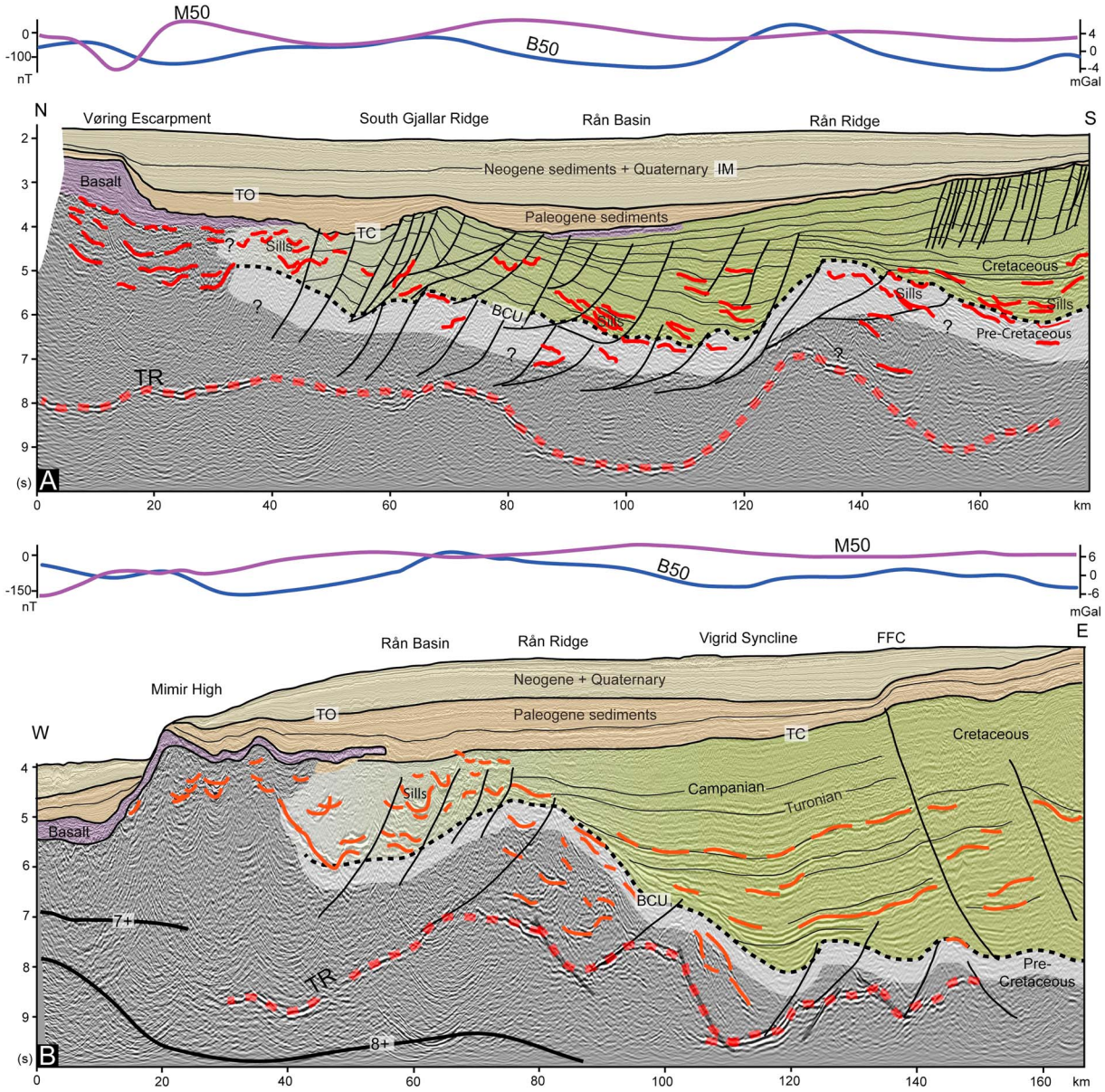

Figure 4. (A) Interpreted seismic section (in two-way travel time) showing the smooth *T*-Reflection along the South Gjallar Ridge, the Rån Basin, and the Rån Ridge. (B) Interpreted seismic section (in two-way travel time) showing the discontinuous *T*-Reflection along the Rån Ridge. The 7+ km/s (considered as top LCB) and the 8+ km/s (the seismic Moho) layers are extracted from refraction data and displayed on the seismic reflection data. Sill intrusions are indicated by thin red lines. The 50 km high-pass filtered gravity (B50) and magnetic (M50) data are plotted above the seismic profiles. BCU: base Cretaceous unconformity; FFC: Fles Fault Complex; IM: intra Miocene; TC: top Cretaceous; TO: top Oligocene; TR: *T*-Reflection. See Figure 6 for line location. Data courtesy from TGS.

Slettringen Ridge (Figure 3B). The *T*-Reflection deepens below the Gleipne Saddle, the Vigrid Syncline, and the Hel Graben where the top is mapped around 9–10 s (Figure 6A).

The *T*-Reflection near the Rån Ridge is more ambiguous and consists of multiple reflections and shows a rough character (Figure 6B). As mentioned by Gernigon et al. (2001), the *T*-Reflection in this area could be correlated with high-velocity basement locally intruded by sills; however, its morphology is characterized by a contrasting and ambiguous faulted geometry (Figure 4B) that differs from the smooth character observed below the South and North Gjallar ridges (Figure 6B). Most of the overlying faults on the Rån Ridge seem to have been active during the Early Cretaceous until the Cenomanian where they terminate and were covered by thick Upper Cretaceous sediments (Figure 4B). Older fault activities that affected the pre-Cretaceous sedimentary succession (Triassic–Jurassic?) are also expected (e.g., Gernigon et al., 2003).

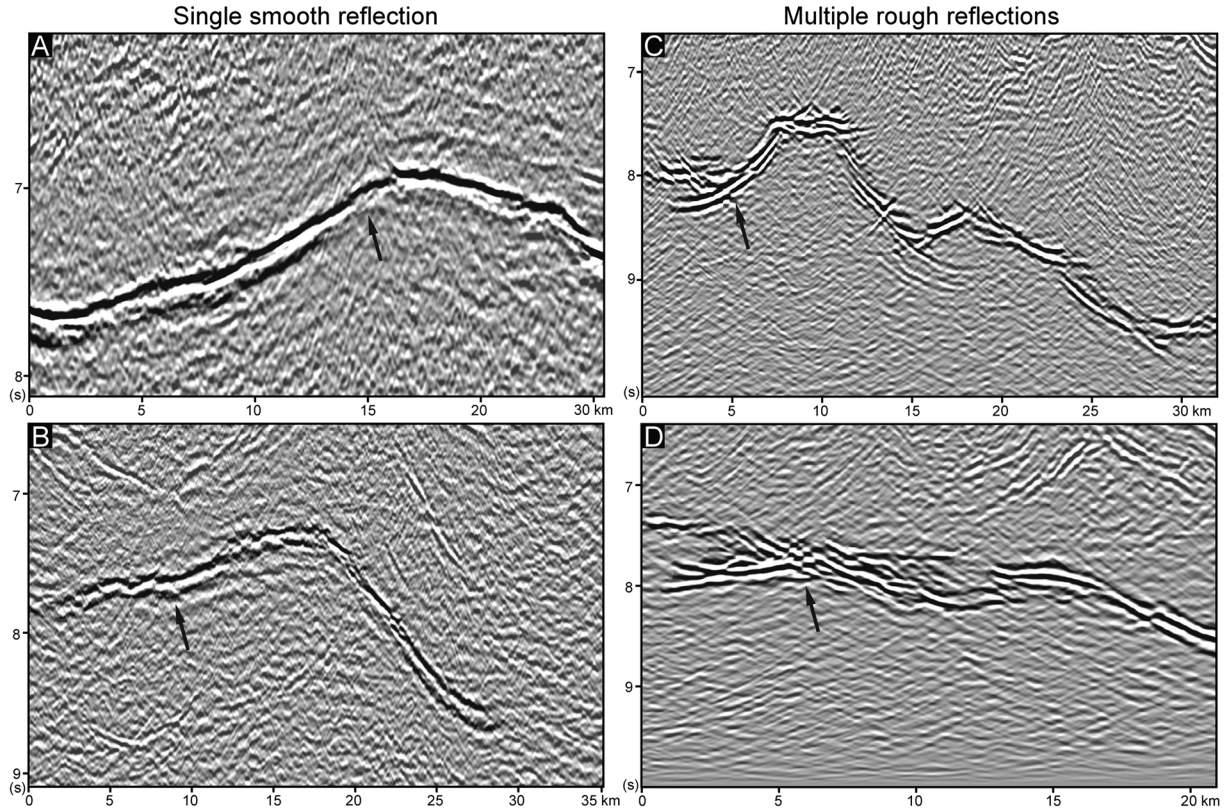

Figure 5. Different shapes for the *T*-Reflection. (A, B) Single reflection and smooth shape. (C, D) Multiple reflections and rough shape. Black arrows indicate the *T*-Reflection. See Figure 6 for lines location.

Locally, the *T*-Reflection seems to be connected to deep sill networks (Figure 7A), with evidence of venting (Figure 7B). Close to Slettringen Ridge, the *T*-Reflection presents a rough shape and may represent the continuation of a preexisting basement high (Figure 7C). The *T*-Reflection often disappears or terminates over fractures and faults (Figure 7D).

By draping the 50 km filtered Bouguer anomaly over the *T*-Reflection topography (Figure 6C), a good correlation is found. Generally, the positive gravity signature corresponds to the different *T*-Reflection domes and highs, whereas the negative filtered Bouguer anomalies correspond to the deeper levels of the *T*-Reflection. The well-defined correlation between the *T*-Reflection and the gravity anomaly confirms that the *T*-Reflection represents a high-impedance boundary associated with a high-density body. No magnetic anomalies are associated with the *T*-Reflection domes on the Vøring Margin (Figure 4). The seismic interpretation also reveals that there is a good correlation between the basin structure (subbasins, highs, and ridges) defined at Cretaceous level and the *T*-Reflection geometry.

4.3. Refraction Data: The LCB Spatial Distribution

From the seismic refraction data (Figure 3A), we compiled maps of the seismic Moho depth (Figure 8A) and the depth (Figure 8B) and thickness of the LCB (Figure 8C). Accordingly, we picked the velocity depth values along individual profiles and created isovelocity maps. The Moho is characterized by isovelocities higher than 8.0–8.3 km/s. The Moho depth along the coast of mainland Norway is tied to Fennoscandia profiles (Breivik et al., 2011; Kinck et al., 1993; Kvarven et al., 2014; Stratford et al., 2009). On the Norwegian mainland, the Moho is about 35 km deep; it becomes slightly shallower below the Vøring and Møre basins (25–27 km), deepens again below the Vøring Marginal High, and rises dramatically toward the oceanic domain (9–15 km) (e.g., Planke et al., 1991). The Moho topography shows an apparent sinistral offset along the Jan Mayen Fracture Zone. The Moho depth increases below the Vøring Spur where thick igneous crust is identified (up to 15 km) and is interpreted to be the result of excess melting along the east Jan Mayen Fracture Zone

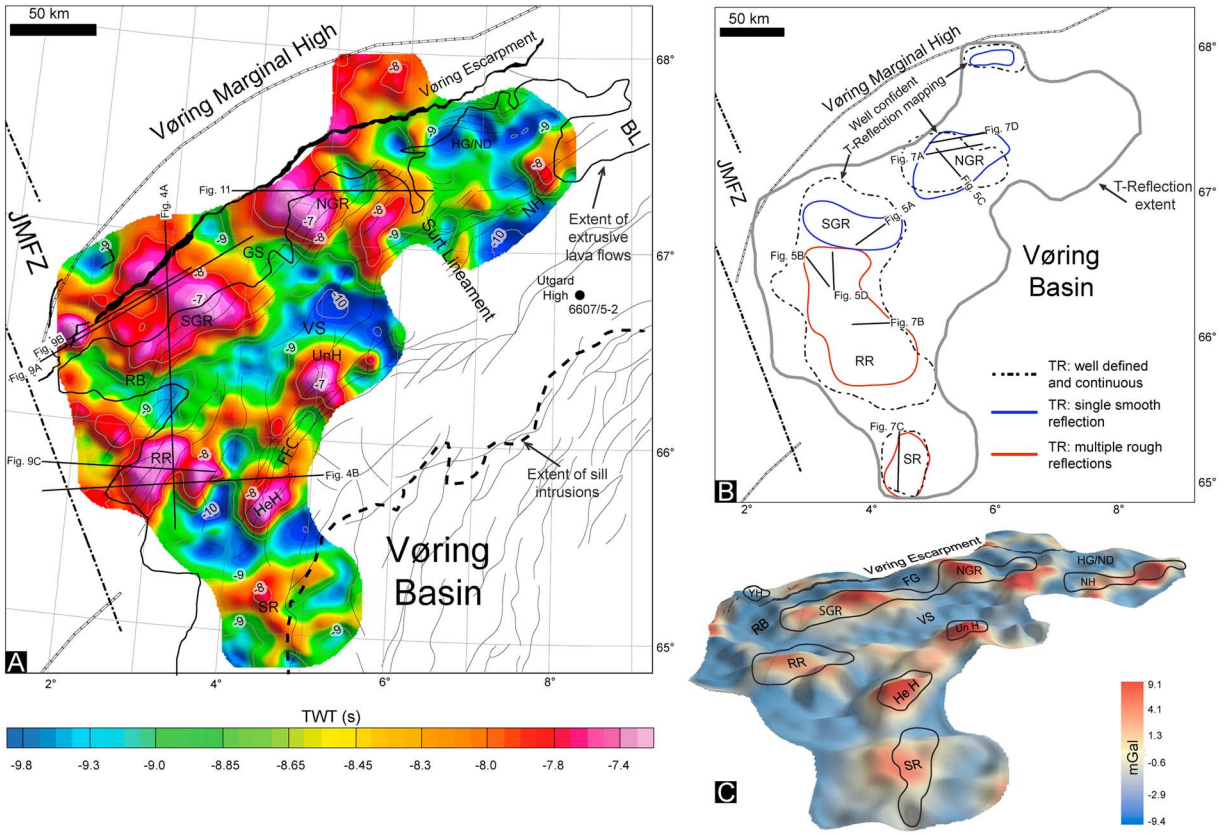

Figure 6. (A) Time-structure map (in two-way travel time) of the *T*-Reflection grid in the Vøring Margin. (B) Shape and character of the *T*-Reflection. (C) 3-D view of the 50 km high-pass filtered Bouguer anomaly draped above the topography of the *T*-Reflection. Thin black lines indicate faults.

during Early–mid-Eocene time (Gernigon et al., 2009), or alternatively during a younger Miocene magmatic event (Breivik et al., 2014).

The top LCB (Figure 8B) is generally defined as the top of the 7+ km/s velocity layer. The top of the LCB is deeper in the Vøring and Møre basins (depths ranging between 18 and 22 km) and becomes shallower toward the oceanic crust (depths ranging between 10 and 12 km). In the oceanic Lofoten Basin, the top LCB is shallower (between 10 and 16 km) compared to the Vøring and Møre margins. For the LCB thickness map (Figure 8C), we considered V_p velocities between 7.1 and 7.7 km/s as criteria to calculate the LCB thickness. We extended our mapping into the oceanic domain, and we defined the outer limit of the LCB where "normal" oceanic crust (6–8 km thickness) was clearly identified at the location of magnetic chrons C22–C23. The thickness of the LCB varies considerably, from 0 to about 8–9 km, which might be caused by variations in the prebreakup structure and/or by the late "magmatic underplating" process that affected the preexisting crust.

On the Vøring Margin, the thickness of the LCB changes along and across the strike of the seismic profiles. Rounded and elongated shaped features, with thicknesses ranging between 6 and 8 km, characterize the Vøring Basin. On the Vøring Marginal High, local increase of LCB thickness to more than 6 km could be correlated with location of the thicker part of the Seaward Dipping Reflectors. Near the Vøring Transform Margin, the LCB is thinner (less than 2 km) and shows a limited extent. On the Møre Margin, our mapping shows a more regular distribution of the LCB thickness. The thicker part (~5 km) is situated beneath the Møre Marginal High and could be correlated with the extent of the Seaward Dipping Reflectors. The LCB thickness decreases oceanward until disappearing west of magnetic chron C23. A local anomaly below the Vigra High is noticed where the LCB reaches a thickness of 4 km. The LCB thickness decreases toward the limit of sill intrusion in the sedimentary basin (Figure 8C). On the Lofoten–Vesterålen Margin, northeast of the Bivrost Lineament, the LCB has a very limited extent. The thicker part (~4 km) is situated along the continent–ocean boundary, and a rapid decrease in thickness is noticed in the oceanic domain toward magnetic chron C23.

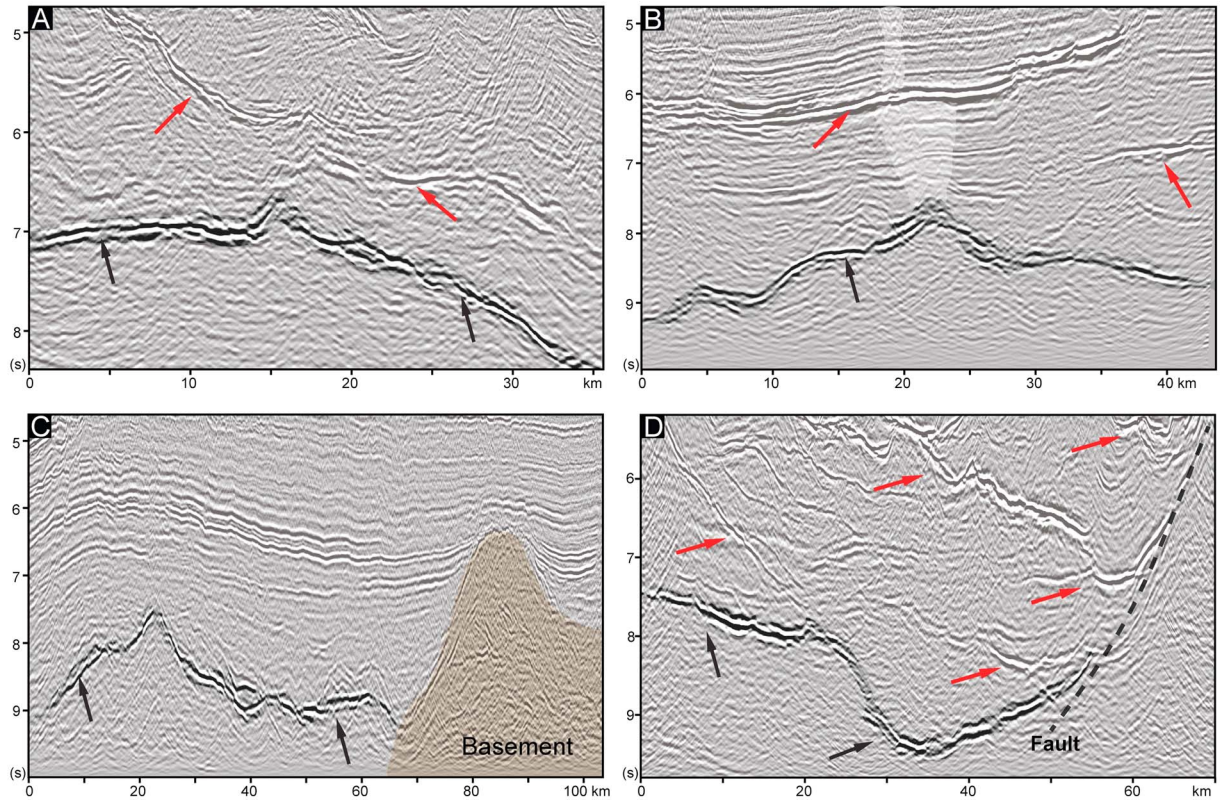

Figure 7. *T*-Reflection and relationship to deep basin structure. (A) Possible connection between *T*-Reflection and the overlying sill network. (B) Possible venting event associated with *T*-Reflection. White shaded area indicates possible venting event. (C) Continuation of the *T*-Reflection at the location of the basement high. (D) The *T*-Reflection terminates along a fault. Black arrows indicate the *T*-Reflection, and red arrows indicate the sill intrusions. We added a transparency around the *T*-Reflection to highlight it in the seismic profile. See Figure 6 for line location.

5. Discussion

5.1. Comparison Between the *T*-Reflection and the LCB Using Seismic Data

The generation of long-offset and high-quality seismic reflection profiles acquired along most of the rifted margins leads to the unraveling of an unexpected variety of structures (e.g., Clerc et al., 2017) and provides unprecedented access to the processes occurring in the middle and lower continental crusts. On the Vøring volcanic margin, offshore mid-Norway, seismic reflection data reveal the existence of strong and laterally continuous reflections referred to as the *T*-Reflection. It has been suggested that the *T*-Reflection on the North Gjallar Ridge matches with the top of the continental part of the LCB (Gernigon et al., 2004); thus, understanding the relationship between the *T*-Reflection and the LCB is of first-order importance to address the deep structure of the margin.

5.1.1. 2-D Comparison

From the time-converted refraction profiles, we have attempted a direct comparison between the seismic reflection and refraction data as illustrated in Figure 9A. The refraction profile 11-96 was shot in a SW–NE direction along the Fenris Graben. The different velocities modeled along the refraction profile are indicated (e.g., Mjelde, Shimamura, et al., 2003). The LCB is indicated by velocities ranging between 7.2 and 7.5 km/s. On the seismic reflection line covering the central part of the refraction profile 11-96, the basaltic layer contributes to an imprecise image of the deeper parts of the sedimentary basin and crustal structure (Figure 9B). The modeled *P* wave velocities allow the identification of different crustal structures (top crystalline basement, LCB, and Moho). Along the refraction profile 11-96, the *T*-Reflection is located at different level (with depths ranging between 8 and 10 s) and displaying different *P* wave velocities. Below the Gleipne Saddle, the *T*-Reflection is deeper than the top of the LCB and shows a level close to the Moho defined by refraction modeling (Figure 9A). Along the Fenris Graben, the *T*-Reflection is located within the LCB layer but often fits

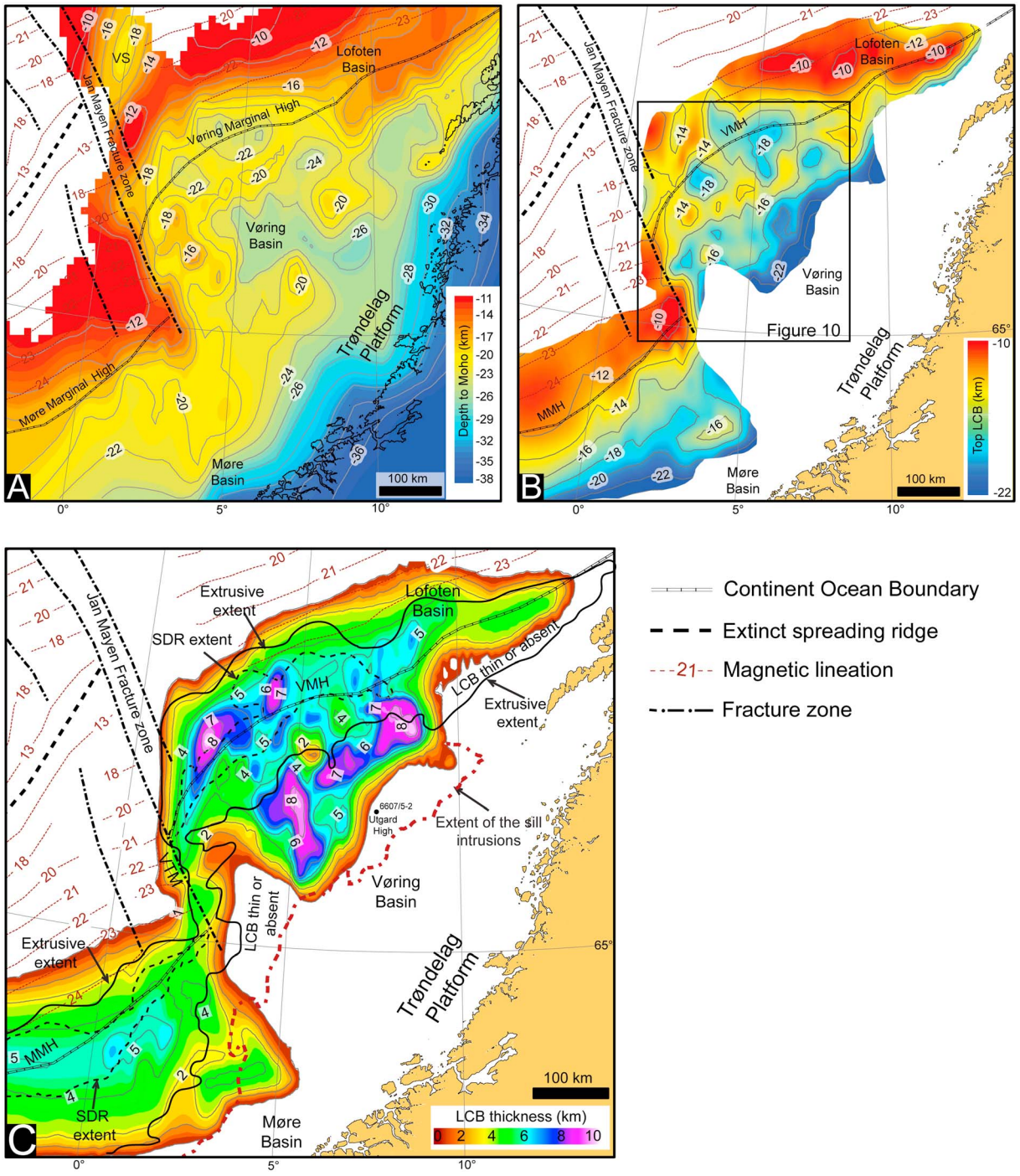

Figure 8. (A) Seismic Moho depth. (B) Top of the Lower Crustal Body (LCB). (C) Thickness map of the LCB. The different maps are compiled and interpolated using all available seismic refraction data. The extrusive extent corresponds to the breakup related volcanics defined from the volcanostratigraphic volcanic facies units. MMH: Møre Marginal High; VMH: Vøring Marginal High; VTM: Vøring Transform Margin; VS: Vøring Spur.

the top of the LCB or is close to it. Along the Rån Ridge, the *T*-Reflection is well defined and can be mapped continuously. On the refraction profile 6-00 (Raum et al., 2006; Figure 9C), the *T*-Reflection is associated with velocities ranging between 5 and 6 km/s. However, *P* wave velocity of 7+ km/s have been modeled at the level of the *T*-Reflection, along the same transect (Rouzo et al., 2006), showing already that OBS modeling can produce a large range of uncertainties.

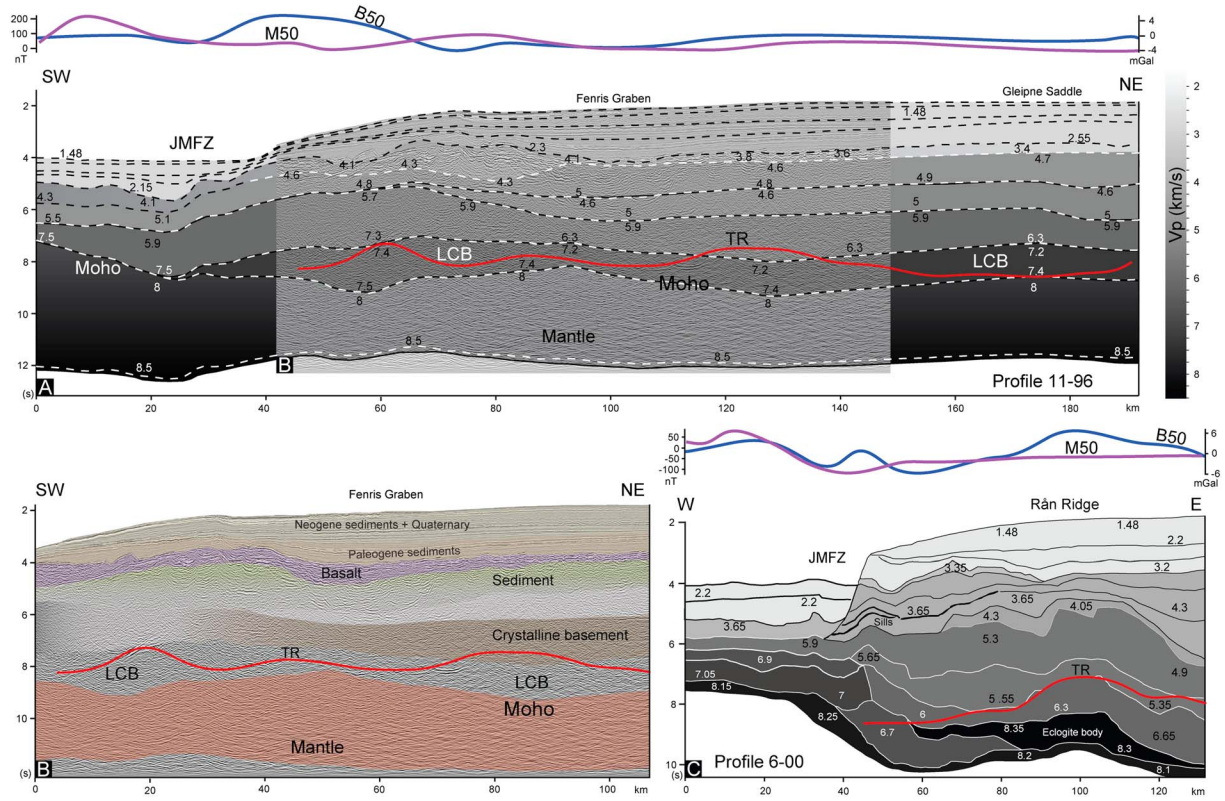

Figure 9. (A) Time-converted refraction profile 11-96 (Mjelde, Shimamura, et al., 2003) overlain by (B) the coincident seismic profile. (C) *T*-Reflection plotted above the refraction profile 6-00 (Raum et al., 2006). The 50 km high-pass filtered gravity (B50) and magnetic (M50) data are plotted above the seismic profiles. TR: *T*-Reflection (red line). See Figure 6 for lines location.

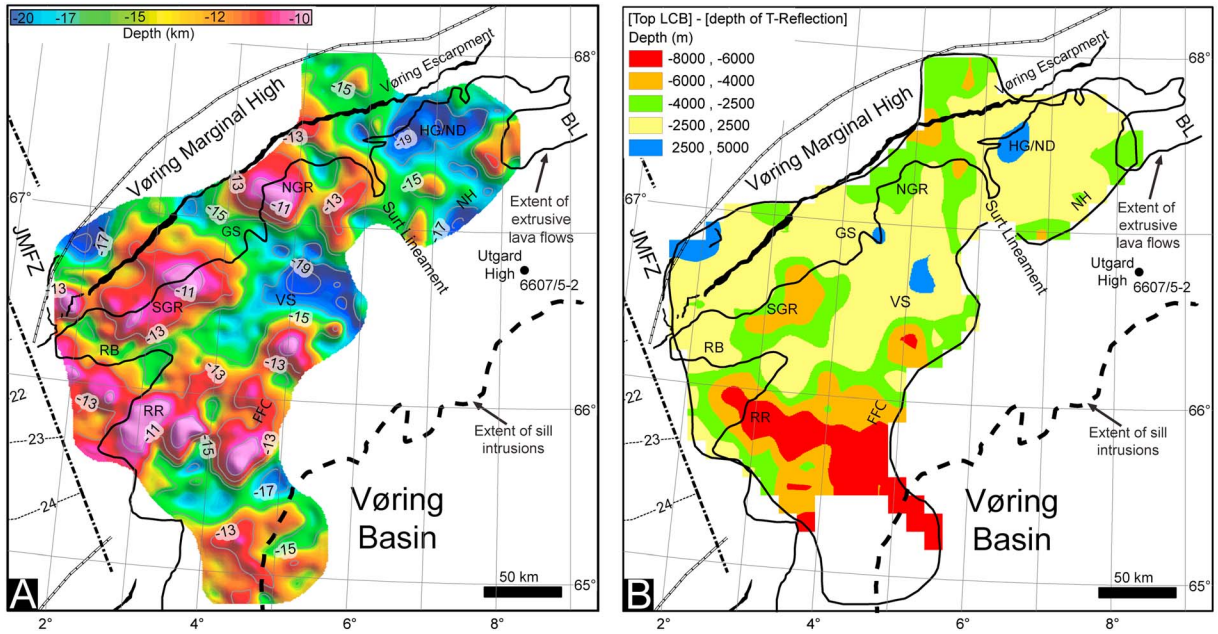

Figure 10. (A) Depth-converted *T*-Reflection. (B) Difference map between top LCB and depth-converted *T*-Reflection. The interval difference showing values ranging between −2500 m and +2500 m (yellow color) correspond to the area where *T*-Reflection and top LCB match. A positive (blue color) or negative (red, orange, and green colors) difference indicates that the *T*-Reflection is deeper or shallower than top LCB, respectively.

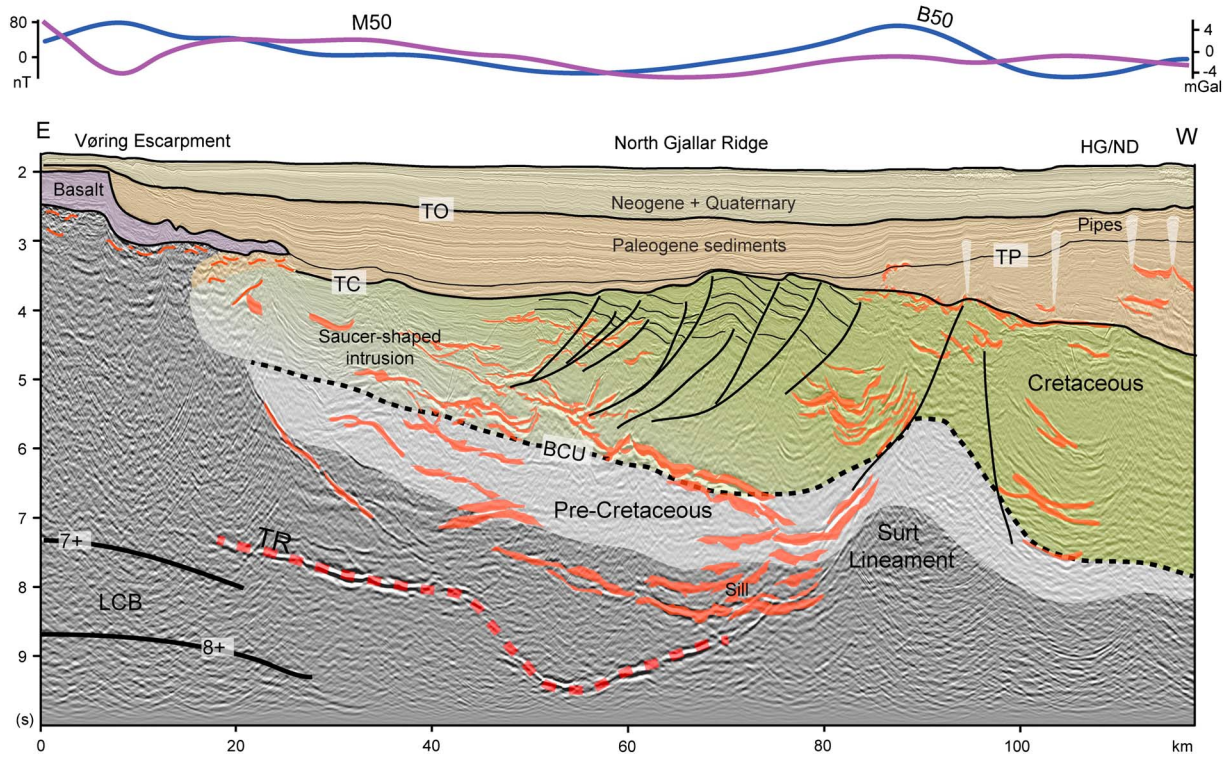

Figure 11. Deep sill network in the Vøring Margin. The 50 km high-pass filtered gravity (B50) and magnetic (M50) data are plotted above the seismic profiles. Different pipe structures are identified and interpreted as hydrothermal vent complexes and seepages. See Figure 6 for location.

5.1.2. 3-D Comparison

The depth-converted seismic data shows that the *T*-Reflection depth ranges between 11 and 19 km in the Vøring Basin (Figure 10A). The *T*-Reflection depth ranges between 11 and 13 km above the North and South Gjallar ridges and the Rån Ridge. A deeper *T*-Reflection, between 13 and 15 km, is interpreted below the Hevring High and the Unn High and deepens in Vigrid Syncline and Hel Graben/Nagfar Dome to 15–19 km.

The difference map between the top LCB and the depth-converted *T*-Reflection is also shown in Figure 10B. Locally, the differences are quite significant and can be explained by uncertainties in the different techniques used in depth conversion (see section 3.2). Nonetheless, we consider an error of ±2500 m when comparing the top LCB compiled from refraction data and the depth-converted *T*-Reflection using stacking velocities (Figure 10B). In this context, the interval with values ranging between −2500 m and +2500 m corresponds to the area where the *T*-Reflection and the top LCB likely match. This area corresponds approximately to 50% of the area where the *T*-Reflection is mapped on the Vøring Margin. In the Vigrid Syncline, the Hel Graben, and the Gleipne Saddle, the mapped *T*-Reflection is generally deeper than the top LCB based on the refraction data. This difference could possibly be related to depth conversion issues especially in the deepest part of the sedimentary basin and basement where the stacking velocities are more uncertain. In the North and South Gjallar ridges, the *T*-Reflection depth mostly corresponds to the top LCB. The *T*-Reflection is shallower than the top LCB in the southwestern corner of the Vøring Basin. In this area, which has been affected by strike-slip tectonic movement, the LCB is thin or absent (Berndt, Mjelde, et al., 2001). Furthermore, high V_p velocities on the Rån Ridge have been interpreted as indication of the existence of a deep seated eclogite body (Figure 9C; e.g., Raum et al., 2006). However, we note that an alternative model suggests that the *T*-Reflection coincides with velocities of up to 7 km/s (Rouzo et al., 2006).

5.2. Spatial Correlation Between Sill Intrusions, *T*-Reflection, and LCB

On the basis of our new observations at the deeper level of seismic profiles, the distribution of deep sill networks becomes clearer. An example of a complex sill network in the Vøring Basin is illustrated in Figure 11. Sills are easily identified by their characteristic high-amplitude seismic response, saucer shape, discordant

reflection geometry, and abrupt terminations (e.g., Planke et al., 2005). They are also associated with hydrothermal vent complexes that were mainly formed by explosive eruptions of gases, liquids, and sediments during sills emplacement (e.g., Svensen et al., 2004). Sills intruded at deeper crustal levels are larger than those identified at shallower levels in terms of both thickness and lateral extent (Figure 11). A characteristic feature is that most of the sills are vertically connected via magmatic junctions (e.g., Cartwright & Hansen, 2006). This observation indicates that individual sills are often interconnected and part of larger sill complexes (e.g., Hansen et al., 2004). In the North Gjallar Ridge, the sill network can be traced vertically from Paleocene sediments down to the *T*-Reflection level inferred to represent the top of the Lower Crustal Body. Wilson and Wheeler (2002) previously inferred a connection between the LCB and the overlying sill complex noting that magma "appears to move from sill to sill via a complex system of narrow, dyke-like feeders.". Fractures and faults may play an important role in magma transfer as it is easier for magma to use a zone of weakness. In Figure 11 an interesting feature can be observed, the sill network appears to terminate against the Surt Lineament and use this weakness zone as a conduit to shallower levels.

In the Vøring Basin, the sedimentary sequences above the LCB are strongly intruded by sills (e.g., Brekke, 2000; Planke et al., 2005), and the concentration of sills appears to be highest in the central part of the basin where the LCB is thicker (e.g., Mjelde, Faleide, et al., 2009). Sills are generally found at their deepest position and lowest stratigraphic levels in the eastern part of the Vøring Basin (e.g., Planke et al., 2005) and typically step up toward the west to their highest levels close to the Vøring Escarpment. However, subsill imaging remains difficult partly due to transmission loss across high-impedance contrast boundaries. Complicating factors, such as offset-dependent tuning, complex 3-D geometries of sills, velocity increases in the metamorphic aureole, and structural variations in the overburden, commonly make it difficult to obtain good resolution criteria (Planke et al., 2005, 2015). It is often possible to interpret several sill intrusions, but the continuity of deeper sills is commonly lost when the thickness and/or number of the overlying sills increases. In addition, high-amplitude seismic events below the uppermost sill are commonly not primary events but rather peg-leg multiples or converted waves (e.g., Berndt et al., 2000).

In the Vøring Basin, exploration well 6607/5-2 at the Utgard High penetrated two microgabbro sills intruded into Upper Cretaceous mudstone and sandstone lithologies (Neumann et al., 2013). Sonic logs from sills show an average velocity of 7 km/s (Planke et al., 2005, 2015). Multichannel seismic reflection profiles in the Hel Graben reveal a sill complex at approximately 5 km depth associated with exceptionally high, 7.4 km/s seismic wide-angle velocities (Berndt et al., 2000). Such velocities are within the velocity range that characterizes the LCB in volcanic passive margins. Interestingly, in the mid-Norwegian margin, the sill extent correlates very well the LCB extent (Figure 8C).

5.3. The Nature of the LCB in the Continental Domain

Unraveling the nature of the LCB is crucial to understand the deep structure and tectonic evolution of the volcanic margins and its implications in terms of crustal thinning, heat flow, and vertical motion. Depending on alternative interpretations, the magmatic rock volume of the North Atlantic large igneous province may be significantly less than previously thought, considering that 60–80% of the volume of this large igneous province has been estimated to reside in the LCB (Eldholm & Grue, 1994; R. S. White et al., 1987).

Refraction data along the Vøring Margin indicates large variations in thickness and velocity within the LCB, which have been proposed to relate to the distribution of mantle melts via feeder dykes (Mjelde et al., 2002). The velocities of this layer vary between 7.0 and 7.7 km/s and have often been interpreted as a function of differences in the magma composition due to inhomogeneities in the asthenospheric source or as a function of mafic differentiation inside the LCB (Mjelde, Raum, Breivik, et al., 2005). The variability in LCB dimensions and velocities demand a consideration of properties in terms of geodynamic setting. First, similarity in LCB velocity ranges does not necessarily imply the same emplacement process and composition. Secondly, temperature–pressure relations may, in some settings, allow secondary metamorphic processes during or subsequent to emplacement.

Geochemical analyses of the Utgard High sills demonstrate that the LCB can be explained as a heterogeneous mixture of cumulates associated with the opening related magmatism and less dense rocks such as old continental basement (Neumann et al., 2013). In this context, the "cumulate" could be defined as a rock that forms via partial crystallization of a melt, after which the remaining melt is removed from the system.

Because igneous cumulates commonly contain more MgO than their parental liquids and because rocks with higher MgO have a higher seismic velocity, cumulate lower crust formed by fractional crystallization should have the highest velocity. This provides an upper limit on the deviation of lower crustal velocity from bulk crustal velocity (e.g., Korenaga et al., 2002).

Wangen et al. (2011) also concluded that a scenario involving a LCB constituting solely of underplated material would require an unrealistic amount of extension. A scenario where underplating or lower crustal intrusion (magmatic addition) accounts for maximum half the LCB is more likely. Berndt et al. (2000) noted that the geophysical expression of the high-velocity mafic lower crust is complex and may alternatively be interpreted as a preexisting crust injected by scattered high-velocity sills. A model involving a mixture of rocks with contrasting physical properties is in agreement with the large variation in V_p (7.1–7.8 km/s) and relatively low V_p/V_s ratios (1.7–1.85) documented within the LCB by Mjelde et al. (2002).

P wave velocities in low-grade crystalline rocks are found to increase from ~6.0 km/s in granite (felsic) to ~6.9 in gabbro (mafic). The V_p/V_s ratio increases correspondingly from ~1.70 to ~1.85 (e.g., Holbrook et al., 1992). Increasing the *P* wave velocity in gabbro to the range observed in the Vøring Basin can be achieved by (1) increasing the temperature of the melt and thereby the MgO content or (2) increasing the metamorphic grade to granulite facies (Hurich et al., 2001). The observed densities, V_p, and V_p/V_s ratios are compatible with both hypotheses.

Lower crustal *P* wave velocities in the range of 7.2–7.6 km/s are also compatible with a crustal layer comprising partly serpentinized peridotites, the existence of which has been postulated in the deeper parts of the Møre Basin (Osmundsen & Ebbing, 2008; Reynisson et al., 2010). Lundin and Doré (2011) proposed that the anomalously wide LCB could have two origins: an inner part made up of partially serpentinized mantle related to Early Cretaceous hyperextension and an outer narrower part of intruded lower crust that overprinted the margin edge during breakup. These authors argued that partial serpentinization (10–30%) can readily account for the *P* wave velocities of the LCB beneath the Cretaceous basin (e.g., Escartín et al., 2001). Partial serpentinization probably takes place during or soon after hyperextension (Skelton et al., 2005), and a LCB formed in this manner would explain a temporal and spatial relationship to the crustal thinning and overlying basin fill.

However, the low V_p/V_s ratios observed on the Vøring Marginal High and in the northern Vøring Basin could be inconsistent with serpentinized peridotites (Mjelde et al., 2002; Mjelde, Raum, et al., 2003). Despite uncertainties about V_p/V_s estimates and interpretations, the authors also argued against the serpentinized peridotite hypothesis in the central and southern Vøring Basin. The existence of clear Moho reflections, *S* wave anisotropy, the absence of *P* wave anisotropy, and low stretching factors do not support the presence of serpentinized mantle. The same conclusion was drawn by Gernigon et al. (2004), primarily based on arguments related to the stretching factors, fault decoupling within the sedimentary formation, and interrogation about the fluid budget. Nirrengarten et al. (2014) and Theissen-Krah et al. (2017) also argued against a serpentinization origin of the LCB in the Møre Margin from 2-D potential field modeling results. Gernigon et al. (2015) suggested that too much continental crust is likely preserved on top of the distal LCB to fit a broad zone of exhumed serpentinized mantle in the outer part of the Møre Margin. A comparison with the distal parts of magma-poor margin (Iberian type) was not easily supported by the data and do not necessarily fit with the long period of rifting and noncontinuum of deformation observed in the mid-Norwegian margin (Gernigon et al., 2015). The correlation between the landward sill extent and the LCB extent is an evidence for a magmatic component in the deeper part of the margin. A serpentinized mantle could not generate sufficient melt to account for the highly intruded sedimentary basin.

Despite limitations, discussion and numerous arguments mentioned above, Peron-Pinvidic and Osmundsen (2016) suggested the presence of a broad zone of exhumed serpentinized mantle directly underneath the lava flows and SDR in the Vøring and Møre marginal highs and presented a magma-poor and ultra-slow spreading scenario to explain the development of the volcanic margin. However, velocities compiled in our study support the presence of thick crystalline basement crust preserved on top of the LCB underneath the Landward Flows and adjacent SDR seismic facies units. The petrology and geochemistry results of the lava flows from ODP Hole 642E also show evidence of continental contamination (Abdelmalak, Meyer, et al., 2016; Meyer et al., 2009) that cannot easily be explained by the presence of a shallow serpentinized mantle lying just underneath the subaerial lava flows. In a similar tectonic setting (Uruguay volcanic margin),

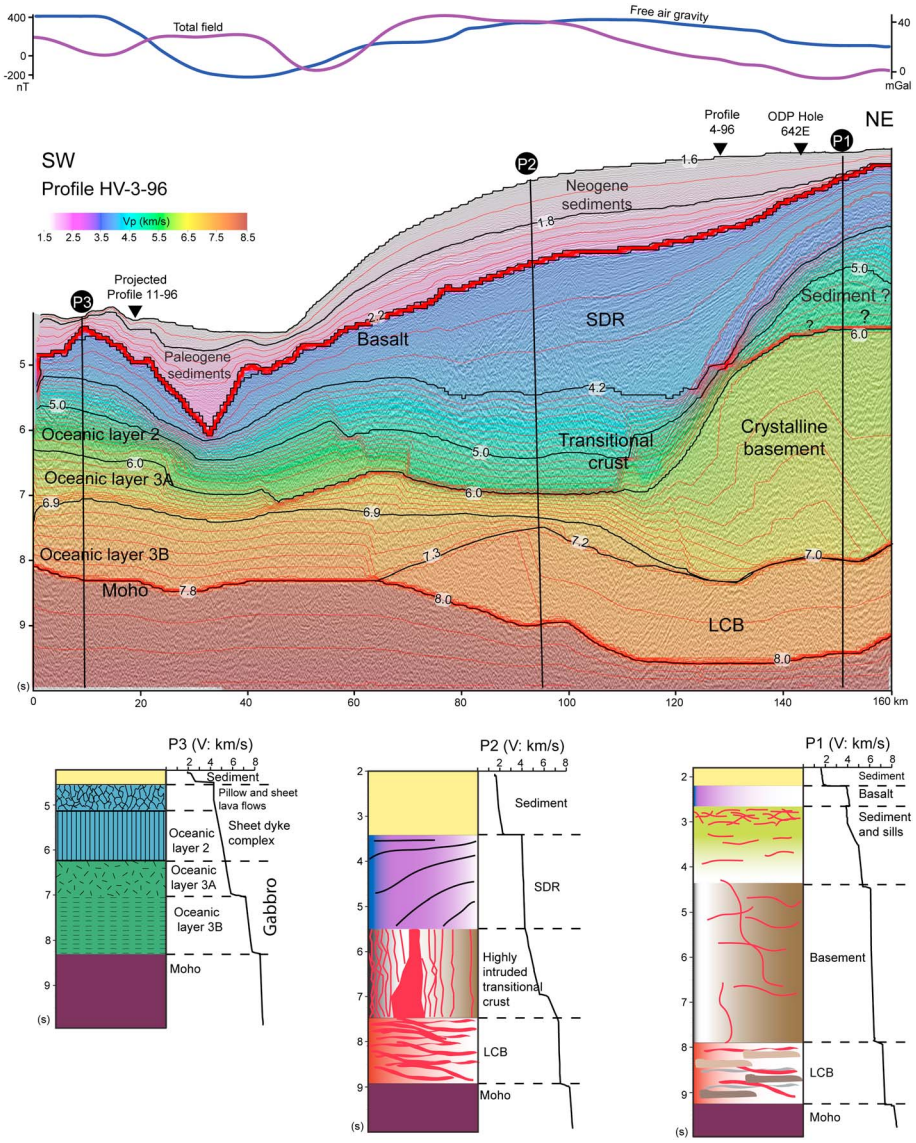

Figure 12. Velocity structure of the continent–ocean transition in the Vøring Margin plotted above the seismic reflection line HV-3-96. The seismic velocity structure is determined using ocean bottom seismometer (OBS) profiles crossing the line (profiles 3-96 and 4-96 (e.g., Mjelde, Shimamura, et al., 2003)) and tied to the Oceanic Drilling Program (ODP) Hole 642E. The total field magnetic and the free air gravity data are plotted above the seismic profiles. Velocity depth profiles for the continental (P1), the continent–ocean transition (P2), and the oceanic (P3) domains are plotted. For each profile the crustal structure is indicated (see section 5.3 for more details and Figure 3A for profile locations).

Clerc et al. (2015) showed evidence that the continental lower crust is most likely preserved underneath the SDR and adjacent basins and also confirm that volcanic margin and magma-poor margins show striking differences (e.g., Clerc et al., 2017; Franke, 2013; Geoffroy et al., 2015).

5.4. The Nature of LCB in the Continent–Ocean Transition and Oceanic Domains

A seismic transect across the continent–ocean transition in the Vøring Margin is shown in Figure 12. On the seismic reflection profile, the top basalt reflection is easily identifiable due to the high-impedance contrast between the postbreakup sediments and the volcanics. The top of the basaltic sequences is an unconformity and correlative conformity between the postbreakup sediments and the underlying basaltic rocks and represents the continentward continuation of the top oceanic basement reflection further west (Abdelmalak, Planke, et al., 2016; Berndt, Planke, et al., 2001; Planke et al., 2000). The SDR wedge is characterized by divergent arcuate reflections with increasing dip in the deeper part.

The *P* wave velocity model shows a narrow continent–ocean transition, followed by thick igneous crust that tapers off toward normal oceanic crust. On the continental side, very close to the SDR wedge, the top of the crystalline basement is a surface obtained by interpolation of the depth at which OBS-derived *P* wave velocities change from values $<$5.5 km/s to values $>$6 km/s, typical of continental crystalline rocks (e.g., Mjelde, Raum, Myhren, et al., 2005; Raum et al., 2002). The crystalline basement is overlain by an intruded sedimentary layer with *P* wave velocities between 4.2 and ~5.5 km/s. Below the crystalline basement near the base of the preserved continental crust, a LCB is identified ($V_p > 7.0$ km/s).

On the oceanic side, postbreakup sediments lie directly above the oceanic basement. From the velocity model, oceanic layer 2 is characterized by *P* wave velocities of ~4 to 6 km/s and is interpreted as pillow lavas (layer 2A, V_p 4–5 km/s) underlain by a sheeted dyke layer (layer 2B, V_p: 5–6 km/s; e.g., Christeson et al., 2007). Oceanic layer 3A is characterized by *P* wave velocities ranging between 6 and 6.7 km/s to 6.9 km/s (e.g., R. S. White et al., 1992). Studies of the oceanic crust demonstrate that the lithology of this middle oceanic layer can vary, depending on the spreading rate when it was formed and on how much deformation affected this layer after that (Dijkstra & Cawood, 2004; Mitchell, 2001). Generally, this layer represents a mixture of mafic intrusive rocks and sheeted dykes in unknown proportion (e.g., W. M. White & Klein, 2014). The lowest oceanic layer, 3B, is characterized by *P* wave velocities of 6.9–7.6 km/s (e.g., R. S. White et al., 1992). Because of these high *P* wave velocities and a high V_p/V_s ratio, Raum et al. (2006) interpreted this layer as gabbroic intrusive rocks. At depth, the model is limited by the crust–mantle boundary (Moho), defined when the *P* wave velocities increase from values of 7.6 km/s to values of 7.9–8 km/s in the oceanic domain and 8.0–8.3 km/s in the continental domain (e.g., Mjelde, Raum, Myhren, et al., 2005).

Igneous crustal thickness of 10 km has been inferred for the Møre Margin (Breivik et al., 2006) and Lofoten Margin (Kodaira et al., 1995). Thicker igneous crust has been proposed in the Vøring Marginal High by Breivik et al. (2009). A reduction in igneous crustal and LCB thicknesses in the oceanic domain and the related melt production shortly after breakup may reflect a changing temperature structure of the residual mantle (Eldholm & Grue, 1994). This is attributed to heat advecting from the system (e.g., R. S. White, 1988) and a change to steady-state sea floor spreading.

A ~40 to 50 km wide COT zone separates the crystalline basement and the oceanic layers 3A and 3B (Figure 12). The transition from continental to oceanic crust is characterized by lateral velocity changes at midcrustal levels near the inner edge of the SDR (e.g., Breivik et al., 2014; Mjelde, Raum, Myhren, et al., 2005). Below the SDR sequences, vertical and inclined reflections are identified and interpreted as the feeder dyke system (Abdelmalak et al., 2015). It has been suggested that this transitional crust resembles oceanic layer 3A (Eldholm & Grue, 1994). It may consist of dykes near the transition with the extrusive volcanics and could represent a gabbroic complex in the lower regions (Zehnder et al., 1990). Layer 3B could be assigned as a lateral continuation of the LCB since these two layers are characterized by similar *P* wave velocities (e.g., Raum et al., 2006).

In the Vøring Margin at the COT, highly intruded lower crust below the SDR wedge was observed in several profiles (Figure 13) and has also been identified in the Faroe Margin in the COT zone below the SDRs (R. S. White et al., 2008; R. S. White & Smith, 2009). Variations in seismic velocity in the LCB may reflect variable percentages of intruded igneous rock into preexisting continental crust. Such highly intruded lower crust has been proposed for accretion models of igneous crust in the context of fast spreading ridges (e.g., Korenaga et al., 2002). Nevertheless, calculated half-spreading rates in the Møre and Vøring Margins during the breakup magmatism time indicate a moderate to slow seafloor spreading process (Breivik et al., 2006, 2009; Gernigon et al., 2015).

5.5. The Relationship Between the *T*-Reflection and the LCB

In the absence of deep drilling, calibration of the lithological composition of rocks at depth very often comes from potential field and seismic refraction studies. Magnetic susceptibility, density, and velocity values (and gradients) are regularly used as conclusive of sedimentary, crystalline, magmatic, or mantle rocks. However, it is also well known that different lithologies, with distinct structural, thermal, and geochemical histories, can correspond to similar sets of geophysical parameters (e.g., Mjelde, Faleide, et al., 2009; Saltus & Blakely, 2011).

In the Vøring Margin, the strong correlation between the high-amplitude *T*-Reflection and the gravity signal (Figure 6C) indicates that the *T*-Reflection represents a high-impedance boundary, for example, between

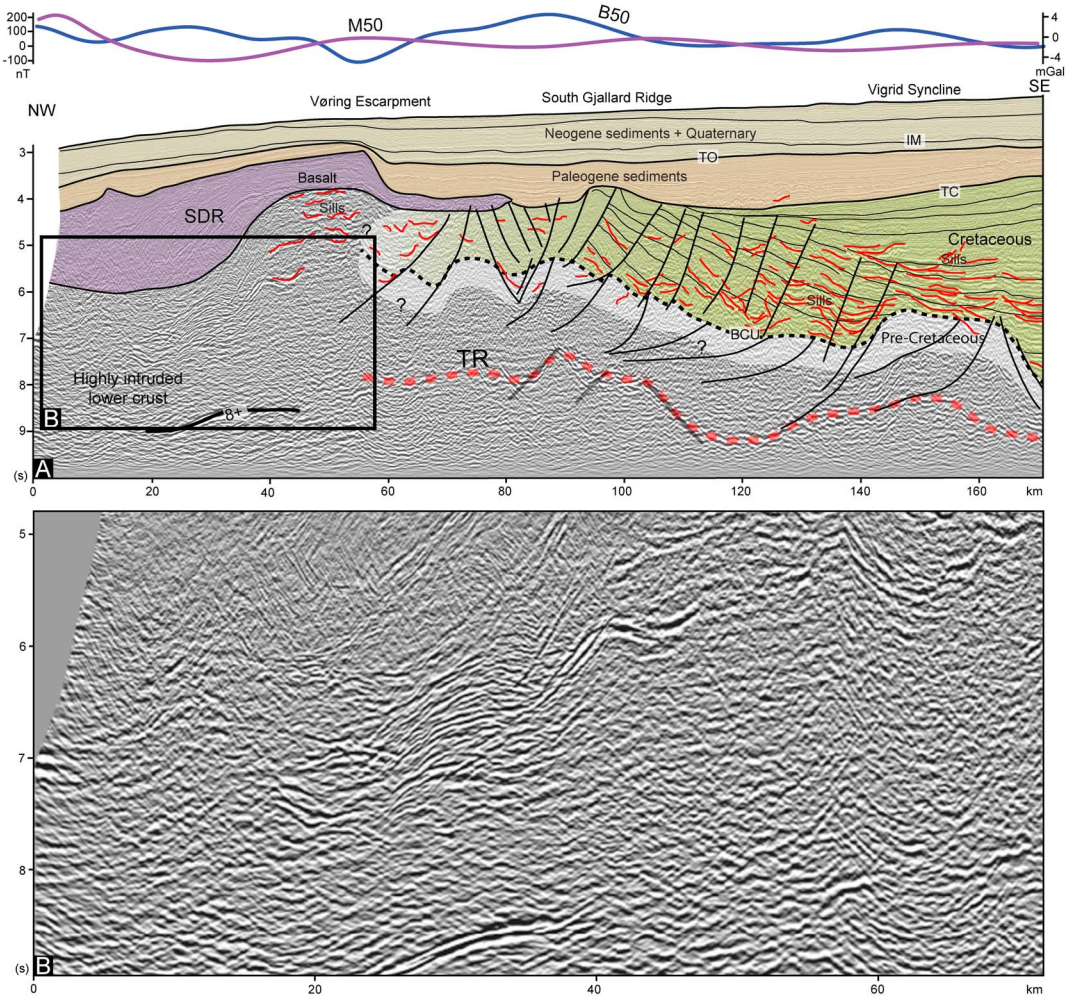

Figure 13. (A) Seismic example along the Vøring Margin showing a highly intruded lower crust below the SDR wedge. The interpretation of the profile is indicated. The 50 km high-pass filtered gravity (B50) and magnetic (M50) data are plotted above the seismic profiles. See Figure 3A for the profile location. (B) Close-up of the highly intruded lower crust below the SDR.

sedimentary rocks and high-density basement rocks such as mid to lower crust or serpentinized mantle (Ren et al., 1998), crustal and underplated gabbroic material (Mjelde et al., 1997, 2002), and/or between upper crustal rocks and high-grade metamorphic rocks such as granulites and eclogites material (Gernigon et al., 2004).

The absence of a magnetic anomaly associated with the dome shape of the *T*-Reflections does not favor a mafic or ultramafic origin (Gernigon et al., 2003, 2004, 2006). From the overall characteristics mentioned above, Gernigon et al. (2006) concluded that the continental part of the LCB observed beneath the outer Vøring Basin may be partly, or fully, attributed to high-pressure granulite/eclogite inherited lower crustal material that is known to display both high *P* wave velocities (7.2–8.5 km/s) and high densities (2.8–3.6 kg/km^3). Raum et al. (2006) and Mjelde, Faleide, et al. (2009) interpreted the lower crust in the southwestern corner of the Vøring Basin as in situ eclogites based on anomalously high *P* wave velocities (8.4 km/s). Such Caledonian eclogite bodies are well documented from western Norway onshore (e.g., Andersen & Jamtveit, 1990), have been inferred from wide-angle seismic data in the lower crust of the mid-Norwegian margin (Kvarven et al., 2014, 2016; Mjelde et al., 2013, 2016; Olafsson et al., 1992), and are also documented offshore East Greenland (Schiffer et al., 2015). High-grade metamorphic rocks are interpreted to have been formed by metamorphism of lower crustal gabbros during the Caledonian orogeny (e.g., Corfu et al., 2014; Kvarven et al., 2014).

All these observations provide a consistent model for preferentially interpreting the *T*-Reflection as the top of an inherited old crystalline, high V_p basement crust, likely to have been exhumed and preserved in the deep part of the rifted margin. Recent modeling suggests that the deep root of the Caledonides can be exhumed

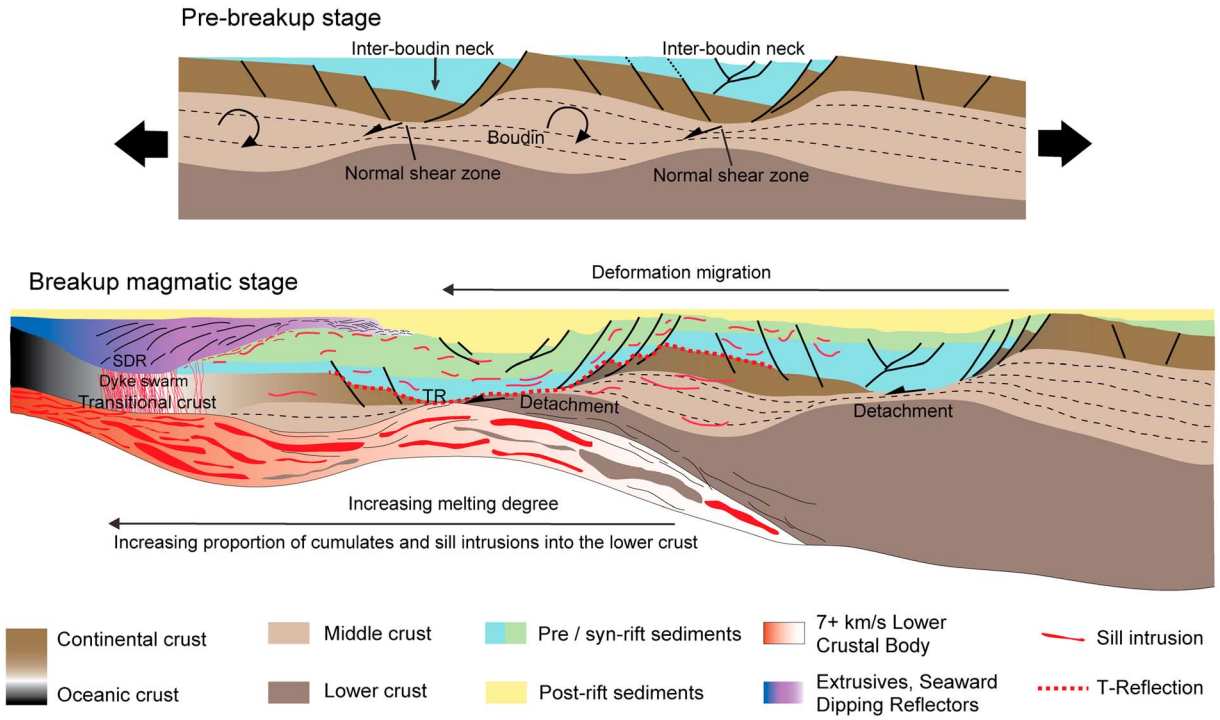

Figure 14. Schematic illustration showing the tectonic evolution of the Vøring Margin before (redrawn after Gartrell, 1997) and during the breakup magmatic stage (see section 5.5 for more details). The crustal structure is characterized by the occurrence of poorly thinned crustal boudins separated by thinned and sheared inter-boudins covered by thick syn-tectonic sediments.

and lie directly underneath the sedimentary basin formed by subsequent rifting of the crust between Norway and Greenland (Petersen & Schiffer, 2016). The dome shape features represented by *T*-Reflection could be the result of an impedance contrast between granulite/eclogitic material, and crystalline rocks and/or metasediments that can be differently compacted and faulted on both sides of a preexisting dome during the deformation of the outer Vøring Basin.

We favor a tectonic scenario (Figure 14) where a large part of the crust observed underneath the pre- and syn-rift sediments could represent both preserved upper continental crustal blocks and middle to lower crustal lenses of inherited and intruded, high-grade metamorphic rocks (e.g., Gernigon et al., 2004). The softening of the crust favored by the high heat flow caused by the igneous rocks may lead to a ductile shearing of the lower crust during extension. As a result, boudinage appears as a recurrent deformation process accounting for the thinning of the continental crust at variable scale (e.g., Clerc et al., 2017; Gartrell, 1997). Consequently, the crustal structure is characterized by the occurrence of rigid crustal blocks, interpreted as thick and poorly thinned crustal blocks, separated by inter-boudins characterized by thinned and sheared crust covered by thick syn-tectonic sediments (Figure 14).

It is well known that the mid-Norwegian margin experienced a prolonged history of extension and basin formation since the collapse of the Caledonian orogeny (e.g., Faleide et al., 2008). The Late Jurassic–Early Cretaceous extension and the Late Cretaceous/Early Paleocene extension are the most important events that led to major fault activity and deep detachments, which in turn control the crustal deformation and subsidence of the margin. Extension formed large-scale rotated rift blocks or structural highs trending NE–SW parallel to weakness zones, probably inherited from the Caledonian crustal configuration. The deep detachments that flattened out at the lower crustal level influenced the development of the sedimentary basin since the drastic thinning phase in Late Jurassic–Early Cretaceous.

Continental breakup between Norway and Greenland occurred in association with a large-scale magmatic activity and volcanism (Eldholm et al., 1989; Skogseid & Eldholm, 1989). Magma intrusion into the lower crust enhanced the metamorphic processes that led to an increasing velocity of the lower crust. The final result was a heterogeneous body made of a mixture of pre- and syn-breakup, and possibly post-breakup, mafic and

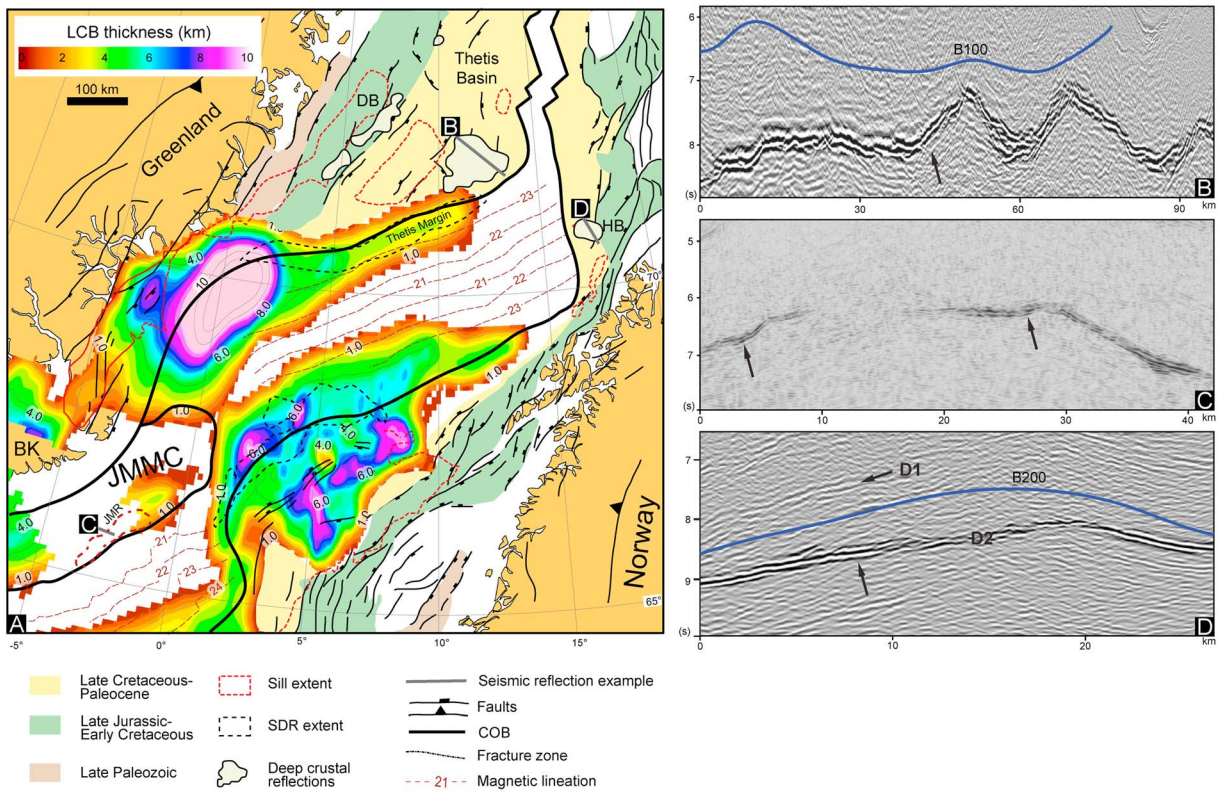

Figure 15. (A) LCB thickness map for the NE Atlantic conjugate margins restored to C21 (~47 Ma) in a fixed Eurasia reference frame using the finite rotations from Gaina et al. (2009). The refraction lines used to compile this map are shown in Figure 1. Examples of deep strong reflections in (B) the NE Greenland margin, (C) the Jan Mayen Ridge, and (D) the SW Barents Sea. Black arrows indicate the deep strong reflection similar to the *T*-Reflection in Norway. The profile location is indicated in Figure 15A. B100 and B200 are the high-pass filtered gravity data with a cutoff of 100 and 200 km, respectively. Seismic interpretation comes from our unpublished data.

ultramafic rocks (cumulates and sills) associated with old metamorphic rocks such as granulites and eclogites. Additionally, the lithological boundary probably also served as favored conduits for igneous intrusions, resulting in the sill-like appearance for parts of the reflections and which may explain the varying reflectivity pattern and the abrupt endings of many of the reflections. Magma may also have intruded the low-angle faults and detachments and top basement contact expected at the level of the *T*-Reflection. The magmatic intrusions may increase the reflectivity of the contacts that appear as very bright reflections on some profiles. This could also be responsible for the local discontinuity of the *T*-Reflection. An increasing melting degree toward the breakup axis is responsible for increasing rate of cumulates and sill intrusions into the lower crust at the COT.

5.6. Lateral Variation Along the Conjugate Margins

To complete the whole picture of the deep structures of the mid-Norwegian margin, we also investigated the NE Greenland conjugate margin (Figure 15). High-quality seismic reflection lines from the NE Greenland margin are sparse but show high-amplitude deep crustal reflections at depths ranging between 7 and 9 s (Figure 15B). These reflections, similar to the *T*-Reflection discussed here, were also mapped beneath the Danmarkshavn Ridge and in the eastern part of the Thetis Basin (Figure 15A). They are discontinuous, show a rough character, and fit with the high-pass filtered Bouguer gravity anomaly. Similar to the *T*-Reflection, the conjugate reflections also represent a high-impedance boundary associated with a high-density body. A strong deep crustal high-amplitude reflection is also found in the Jan Mayen Ridge at depths ranging between 7 and 8 s (Figure 15C). A double midcrustal dome-shaped feature with high-amplitude reflections (named D1 and D2) is found at depths ranging between 7 and 10 s in the Harstad Basin situated in the SW Barents Sea (Figure 15D). The high-pass filtered Bouguer anomaly correlates very well with the doming of

these two deep crustal reflections, which also have no obvious magnetic signature. The main density contrast is likely across D2, whereas D1 is possibly an intra-Jurassic reflection (Figure 15D).

Compared to the mid-Norwegian Margin, the density of refraction lines along the NE Greenland and the Jan Mayen Micro-Continent is lower, and therefore, the shape and the variation of the LCB are not as well constrained. However, seismic refraction data reveal the existence of LCB along the NE Greenland margins (Hermann, 2013; Mandler & Jokat, 1998; Schlindwein & Jokat, 2000; Schmidt-Aursch & Jokat, 2005; Voss & Jokat, 2007; Voss et al., 2009; Weigel et al., 1995). From the available refraction data (Figure 3A), we also compiled the LCB thickness map along the NE Greenland margin (Figure 15A) and find it thicker than at the mid-Norwegian margin. The thicker part (12–15 km) of the LCB is situated below the Foster Volcanic Province, and it becomes thinner below the Jameson Land where sill intrusions but no volcanic extrusives are found. Along the Thetis Margin, the thickness of the LCB does not exceed 4 km. Similarly to the mid-Norwegian margin, the LCB thickness decreases at magnetic chrons C23–C22 and merges into oceanic layer 3. A high-velocity lower crust, with V_p of more than 7 km/s, is also identified in the eastern margin of the Jan Mayen Micro-Continent (Breivik et al., 2012).

Offshore NE Greenland, two igneous sill complexes are identified in the Thetis Basin and the Danmarkshavn Basin (e.g., Reynolds et al., 2017). The sill complex of the Danmarkshavn Basin is continuous landward until the Jameson Land area (Figure 15A). If we consider a link between the igneous sill complexes and the extent of the LCB, we expect that the latter should be present below the Thetis and the Danmarkshavn basins. Such an assumption could only be verified by new refraction data. We estimated the total extent of the LCB and its volume for the Vøring–Lofoten and NE Greenland conjugate margins. We considered a fully magmatic LCB, which is therefore an overestimation (see discussion above) and thus represents a maximum of melt production. For the NE Greenland area, the LCB covers an area of ~136,000 km^2 and indicates a maximum volume of 0.56×10^6 km^3. On the conjugate Vøring–Lofoten margins, the LCB covers a similar area of ~140,000 km^2 and indicates a maximum volume of 0.50×10^6 km^3, which is arguably surprising if we consider the asymmetry of the NE Atlantic margins.

6. Conclusions

In this paper we investigated the deep structure of the Vøring Margin offshore mid-Norway using an integrated multidisciplinary geophysical data sets, including reflection and refraction seismic, gravity, and magnetic data. This detailed analysis has resulted in the following conclusions:

1. New seismic data permit a refined mapping of the *T*-Reflection in the outer Vøring Margin. The *T*-Reflection is identified between 7 and 10 s and sometimes consists of one single smooth reflection, such as in the North and South Gjallar ridges. However, it is frequently associated with a set of rough multiple reflections and displays discontinuous steep and flat segments with varying geometries, amplitudes, and contact relationships. The *T*-Reflection seems to be connected to deep sill networks and locally located at the continuation of basement high structures or terminates over fractures and faults.
2. The positive correlation between the geometries of the 50 km high-pass filtered Bouguer anomaly and the *T*-Reflection indicates that the latter represents a high-impedance boundary associated with a high-density body. However, no significant magnetic anomaly is associated with the *T*-Reflection.
3. A comparison between the *T*-Reflection and the top LCB depths, deduced from independent seismic reflection and refraction results, indicates that these two features are found at the same depth (within the uncertainties) in ~50% of the outer Vøring Margin areas.
4. We present a tectonic scenario where a large part of the deep crustal structure is composed of preserved upper continental basement and middle to lower crustal lenses of inherited and intruded high-grade metamorphic rocks. Intrusions into faulted crustal blocks are responsible for the rough character of the *T*-Reflection whereas sill intrusion into the preexisting lower crust and detachment faults could explain the smooth character of the *T*-Reflection.
5. Magma intrusion into the lower crust might be responsible for metamorphic processes that may have led to an increased velocity of the lower crust. The result is a heterogeneous LCB made of a mixture of pre- and syn-breakup mafic and ultramafic rocks (sills and cumulates) associated with older metamorphic rocks such as granulites and eclogites. The positive correlation between the extent, continuity, and lateral thickness variation of the LCB and sill intrusion in the basin is an argument in favor of a breakup magmatic

origin of the LCB. An increased degree of melting toward the breakup axis is likely responsible for an oceanward increase in volumes of cumulates and sill intrusions into the lower crust.

6. Similar domal shapes and high-amplitude reflections associated with high gravity and low magnetic anomalies have been identified on other NE Atlantic margins. However, further investigations are probably required to understand their nature and their possible correlation with the mid-Norwegian margin *T*-Reflection.

Acknowledgments
Funding for this work came from the OMNIS Project: Offshore Mid-Norway: Integrated Margin and Basin Studies (project 210429) funded by the Research Council of Norway through its Centres of Excellence funding scheme, project 223272 CEED (Centre for Earth Evolution and Dynamics). The seismic, magnetic, and gravity data presented in this study were provided by TGS. We would like to acknowledge First Geo AS and TGS for the use of Hiqbe™ regional velocity cube employed in depth conversion of the seismic profiles. Seismic interpretation was done using IHS: Kingdom software. Grid interpolations and map compilations were established using Geosoft Oasis Montaj and ArcGis softwares. GES acknowledges VISTA—a basic research program in collaboration between The Norwegian Academy of Science and Letters, and Statoil (project 6268, "DEFMOD"). We thank Camille Clerc, Christian Schiffer, the associated Editor, and the Editor Claudio Faccenna for useful comments and suggestions that improved the paper.

References

Abdelmalak, M. M. (2010). Transition Spatio-temporelle entre rift sédimentaire et marge passive volcanique: l'exemple de la Baie de Baffin, Centre Ouest Groenland, (Spatio-temporal transition between a sedimentary basin to a volcanic passive margin: The Baffin Bay case example, central west Greenland) (pp. 266). [Available at Université du Maine (France) Retrieved from http://cyberdoc.univ-lemans.fr/theses/2010/2010LEMA1030.pdf, Le Mans].

Abdelmalak, M. M., Andersen, T. B., Planke, S., Faleide, J. I., Corfu, F., Tegner, C., … Myklebust, R. (2015). The ocean–continent transition in the mid-Norwegian margin: Insight from seismic data and an onshore Caledonian field analogue. *Geology*, *43*, 1011–1014. https://doi.org/10.1130/G37086.1

Abdelmalak, M. M., Faleide, J. I., Planke, S., Theissen-Krah, S., Zastrozhnov, D., Breivik, A. J., … Myklebust, R. (2014). Breakup magmatism style on the North Atlantic Igneous Province: Insight from Mid-Norwegian volcanic margin. Paper presented at EGU General Assembly Conference Abstracts, Vienna.

Abdelmalak, M. M., Geoffroy, L., Angelier, J., Bonin, B., Callot, J. P., Gélard, J. P., & Aubourg, C. (2012). Stress fields acting during lithosphere breakup above a melting mantle: A case example in West Greenland. *Tectonophysics*, *581*, 132–143. https://doi.org/10.1016/j.tecto.2011.11.020

Abdelmalak, M. M., Meyer, R., Planke, S., Faleide, J. I., Gernigon, L., Frieling, J., … Myklebust, R. (2016). Pre-breakup magmatism on the Vøring Margin: Insight from new sub-basalt imaging and results from Ocean Drilling Program Hole 642E. *Tectonophysics*, *675*, 258–274. https://doi.org/10.1016/j.tecto.2016.02.037

Abdelmalak, M. M., Planke, S., Faleide, J. I., Jerram, D. A., Zastrozhnov, D., Eide, S., & Myklebust, R. (2016). The development of volcanic sequences at rifted margins: New insights from the structure and morphology of the Vøring Escarpment, mid-Norwegian margin. *Journal of Geophysical Research: Solid Earth*, *121*, 5212–5236. https://doi.org/10.1002/2015JB012788

Andersen, T. B., & Jamtveit, B. (1990). Uplift of deep crust during orogenic extensional collapse: A model based on field studies in the Sogn-Sunnfjord Region of western Norway. *Tectonics*, *9*(5), 1097–1111. https://doi.org/10.1029/TC009i005p01097

Berndt, C. (2002). Residual Bouguer satellite gravity anomalies reveal basement grain and structural elements of the Vøring Margin, off Norway. *Norwegian Journal of Geology*, *82*, 31–36.

Berndt, C., Mjelde, R., Planke, S., Shimamura, H., & Faleide, J. I. (2001). Controls on the tectono-magmatic evolution of a volcanic transform margin: The Vøring Transform Margin, NE-Atlantic. *Marine Geophysical Researches*, *22*(3), 133–152.

Berndt, C., Planke, S., Alvestad, E., Tsikalas, F., & Rasmussen, T. (2001). Seismic volcanostratigraphy of the Norwegian margin: Constraints on tectonomagmatic break-up processes. *Journal of the Geological Society*, *158*(3), 413–426. https://doi.org/10.1144/jgs.158.3.413

Berndt, C., Skogly, O. P., Planke, S., Eldholm, O., & Mjelde, R. (2000). High-velocity breakup-related sills in the Vøring Basin, off Norway. *Journal of Geophysical Research*, *105*, 28,443–428,454.

Blystad, P., Brekke, H., Færseth, R. B., Larsen, B. T., Skogseid, J., & Tørudbakken, B. (1995). Structural elements of the Norwegian continental shelf Part II: The Norwegian sea region, *NPD-Bulletin, The Norwegian Petroleum Directorate*., *8*.

Breivik, A., Faleide, J. I., Mjelde, R., Flueh, E., & Murai, Y. (2014). Magmatic development of the outer Vøring Margin from seismic data. *Journal of Geophysical Research: Solid Earth*, *119*, 6733–6755. https://doi.org/10.1002/2014JB011040

Breivik, A. J., Faleide, J. I., Mjelde, R., & Flueh, E. R. (2009). Magma productivity and early seafloor spreading rate correlation on the northern Vøring Margin, Norway—Constraints on mantle melting. *Tectonophysics*, *468*(1–4), 206–223. https://doi.org/10.1016/j.tecto.2008.09.020

Breivik, A. J., Mjelde, R., Faleide, J. I., & Murai, Y. (2006). Rates of continental breakup magmatism and seafloor spreading in the Norway Basin–Iceland plume interaction. *Journal of Geophysical Research*, *111*, B07102. https://doi.org/10.1029/2005JB004004

Breivik, A. J., Mjelde, R., Faleide, J. I., & Murai, Y. (2012). The eastern JanMayen microcontinent volcanic margin. *Geophysical Journal International*, *188*(3), 798–818.

Breivik, A. J., Mjelde, R., Raum, T., Faleide, J. I., Murai, Y., & Flueh, E. R. (2011). Crustal structure beneath the Trøndelag Platform and adjacent areas of the mid-Norwegian margin, as derived from wide-angle seismic and potential field data. *Norweian Journal of Geology*, *90*, 141–161.

Brekke, H. (2000). The tectonic evolution of the Norwegian Sea Continental Margin with emphasis on the Vøring and Møre Basins. *Geological Society, London, Special Publications*, *167*(1), 327–378. https://doi.org/10.1144/gsl.sp.2000.167.01.13

Brooks, C. K. (2011). The East Greenland rifted volcanic margin. *Geological Survey of Denmark and Greenland Bulletin*, *24*, 96.

Brune, S., Heine, C., Clift, P. D., & Pérez-Gussinyé, M. (2017). Rifted margin architecture and crustal rheology: Reviewing Iberia–Newfoundland, Central South Atlantic, and South China Sea. *Marine and Petroleum Geology*, *79*, 257–281. https://doi.org/10.1016/j.marpetgeo.2016.10.018

Cartwright, J., & Hansen, D. M. (2006). Magma transport through the crust via interconnected sill complexes. *Geology*, *34*(11), 929–932. https://doi.org/10.1130/g22758a.1

Christeson, G. L., McIntosh, K. D., & Karson, J. A. (2007). Inconsistent correlation of seismic layer 2a and lava layer thickness in oceanic crust. *Nature*, *445*(7126), 418–421. http://www.nature.com/nature/journal/v445/n7126/suppinfo/nature05517_S1.html

Clerc, C., Jolivet, L., & Ringenbach, J. C. (2015). Ductile extensional shear zones in the lower crust of a passive margin. *Earth and Planetary Science Letters*, *431*, 1–7. https://doi.org/10.1016/j.epsl.2015.08.038

Clerc, C., Ringenbach, J.-C., Jolivet, L., & Ballard, J.-F. (2017). Rifted margins: Ductile deformation, boudinage, continentward-dipping normal faults and the role of the weak lower crust. *Gondwana Research*. https://doi.org/10.1016/j.gr.2017.04.030

Coffin, M. F., & Eldholm, O. (1994). Large igneous provinces: Crustal structure, dimensions and external consequence. *Reviews of Geophysics*, *32*, 1–36.

Corfu, F., Andersen, T. B., & Gasser, D. (2014). The Scandinavian Caledonides: Main features, conceptual advances and critical questions. *Geological Society, London, Special Publications*, *390*(1), 9–43. https://doi.org/10.1144/sp390.25

Corseri, R., Senger, K., Selway, K., Abdelmalak, M. M., Planke, S., & Jerram, D. (2017). Magnetotelluric evidence for massive sulphide mineralization in intruded sediments of the outer Vøring Basin, mid-Norway. *Tectonophysics*, *706-707*, 196–205. https://doi.org/10.1016/j.tecto.2017.04.011

Dijkstra, A. H., & Cawood, P. A. (2004). Base-up growth of ocean crust by multiple phases of magmatism: Field evidence from Macquarie Island. *Journal of the Geological Society*, *161*(5), 739–742. https://doi.org/10.1144/0016-764904-033

Doré, A. G., Lundin, E. R., Jensen, L. N., Birklamd, Ø., Eliassen, P. E., & Fichler, C. (1999). Principal tectonic events in the evolution of the northwest European Atlantic margin. *Geological Society, London, Petroleum Geology Conference Series*, *5*, 41–61. https://doi.org/10.1144/0050041

Ebbing, J., Lundin, E., Olesen, O., & Hansen, E. K. (2006). The mid-Norwegian margin: A discussion of crustal lineaments, mafic intrusions, and remnants of the Caledonian root by 3D density modelling and structural interpretation. *Journal of the Geological Society, London*, *163*, 47–59.

Eldholm, O., Gladczenko, T. P., Skogseid, J., & Planke, S. (2000). Atlantic volcanic margins: A comparative study. In A. E. A. Nottvedt (Ed.), *Dynamics of the Norwegian margin*, *Spetial Publications* (pp. 411–428). London: Geological Society.

Eldholm, O., & Grue, K. (1994). North Atlantic volcanic margins: Dimensions and production rates. *Journal of Geophysical Research*, *99*, 2955–2968.

Eldholm, O., Thiede, J., & Taylor, E. (1989). Evolution of the Vøring Volcanic Margin. In O. Eldholm, et al. (Eds.), *Proceedings of the ODP, Scientific Results 104* (pp. 1033–1065). College Station, TX: Ocean Drilling Program.

England, P. C. (1983). Constraints on extension of continental lithosphere. *Journal of Geophysical Research*, *88*, 1145–1152.

Ernst, R. E., Buchan, K. L., & Palmer, H. C. (1995). Giant dyke swarms: Characteristics, distribution and geotectonic applications. In G. Baer & A. Heimann (Eds.), *Physics and chemistry of dykes* (pp. 3–21). Rotterdam: Balkerna.

Escartín, J., Hirth, G., & Evans, B. (2001). Strength of slightly serpentinized peridotites: Implications for the tectonics of oceanic lithosphere. *Geology*, *29*(11), 1023–1026. https://doi.org/10.0.4.106/0091-7613(2001)029%3C1023:sosspi%3E2.0.co;2

Faleide, J. I., Tsikalas, F., Breivik, A. J., Mjelde, R., Ritzmann, O., Engen, Ø., … Eldholm, O. (2008). Structure and evolution of the continental margin off Norway and the Barents Sea. *Episodes*, *31*(1), 82–91.

Fichler, C., Odinsen, T., Rueslåtten, H., Olesen, O., Vindstad, J. E., & Wienecke, S. (2011). Crustal inhomogeneities in the northern North Sea from potential field modeling: Inherited structure and serpentinites?. *Tectonophysics*, *510*(1), 172–185. https://doi.org/10.1016/j.tecto.2011.06.026

Franke, D. (2013). Rifting, lithosphere breakup and volcanism: Comparison of magma-poor and volcanic rifted margins. *Marine and Petroleum Geology*, *43*, 63–87. https://doi.org/10.1016/j.marpetgeo.2012.11.003

Gaina, C., Gernigon, L., & Ball, P. (2009). Palaeocene–Recent plate boundaries in NE Atlantic and formation of the Jan Mayen microcontinent. *Journal of the Geological Society of London*, *166*, 601–616.

Gartrell, A. P. (1997). Evolution of rift basins and low-angle detachments in multilayer analog models. *Geology*, *25*(7), 615–618.

Geissler, W. H., Gaina, C., Hopper, J. R., Funck, T., Blischke, A., Arting, U., … Abdelmalak, M. M. (2016). Seismic volcanostratigraphy of the NE Greenland continental margin. *Geological Society, London, Special Publications*, *447*. https://doi.org/10.1144/sp447.11

Geoffroy, L. (2005). Volcanic passive margins. *Comptes Rendus Géosciences*, *337*, 1395–1408.

Geoffroy, L., Burov, E. B., & Werner, P. (2015). Volcanic passive margins: Another way to break up continents. *Scientific Reports*, *5*, 14828. https://doi.org/10.1038/srep14828

Gernigon, L., Blischke, A., Nasuti, A., & Sand, M. (2015). Conjugate volcanic rifted margins, sea-floor spreading and microcontinent: Insights from new high-resolution aeromagnetic surveys in the Norway Basin. *Tectonics*, *34*, 907–933. https://doi.org/10.1002/2014TC003717

Gernigon, L., Lucazeau, F., Brigaud, F., Ringenbach, J.-C., Planke, S., & Le Gall, B. (2006). A moderate melting model for the Vøring Margin (Norway) based on structural observations and a thermo-kinematical modelling: Implication for the meaning of the lower crustal bodies. *Tectonophysics*, *412*(3-4), 255–278.

Gernigon, L., Olesen, O., Ebbing, J., Wienecke, S., Gaina, C., Mogaard, J. O., … Myklebust, R. (2009). Geophysical insights and early spreading history in the vicinity of the Jan Mayen Fracture Zone, Norwegian–Greenland Sea. *Tectonophysics*, *468*(1-4), 185–205.

Gernigon, L., Ringenbach, J. C., Planke, S., Jonquet-Kolstø, E., Ballard, J. F., & Le Gall, B. (2001). Rifting and segmentation along the outer Vøring Basin, North Atlantic margin, Norway. In *American Association of Petroleum Geologists (AAPG) annual meeting* (pp. 1–7). Denver, CO.

Gernigon, L., Ringenbach, J.-C., Planke, S., & Jonquet-Kolsto, H. (2003). Extension, crustal structure and magmatism at the outer Voring Basin, Norwegian margin. *Journal of the Geological Society of London*, *160*, 197–208.

Gernigon, L., Ringenbach, J.-C., Planke, S., & Le Gall, B. (2004). Deep structures and breakup along volcanic rifted margins: Insights from integrated studies along the outer Vøring Basin (Norway). *Marine and Petroleum Geology*, *21*(3), 363–372.

Gradstein, F. M., Ogg, J. G., Schmitz, M. D., & Ogg, G. M. (2012). The Geologic time scale 2012.

Hansen, D. M., Cartwright, J. A., & Thomas, D. (2004). 3D seismic analysis of the geometry of igneous sills and sill junction relationships. *Geological Society, London, Memoirs*, *29*(1), 199–208. https://doi.org/10.1144/gsl.mem.2004.029.01.19

Hermann, T. (2013). The northeast Greenland Margin tectonic evolution (pp. 170). vorgelegt dem Rat der Chemisch-Geowissenschaftlichen Fakultät der Friedrich-Schiller-Universität Jena.

Hinz, K. (1981). Hypothesis on terrestrial catastrophes: Wedges of very thick oceanward dipping layers beneath passive margins—Their origin and palaeoenvironement significance. *Geologisches Jahrbuch*, *22*, 345–363.

Holbrook, W. S., Larsen, H. C., Korenaga, J., Dahl-Jensen, T., Reid, I. D., Kelemen, P. B., … Detrick, R. S. (2001). Mantle thermal structure and active upwelling during continental breakup in the North Atlantic. *Earth and Planetary Science Letters*, *190*, 251–266.

Holbrook, W. S., Mooney, W. D., & Christensen, N. J. (1992). The seismic velocity structure of the deep continental crust. In R. A. D. M. Fountain & R. W. Kay (Eds.), *Continental lower crust, development in geotectonics* (pp. 1–43). Amsterdam: Elsevier.

Huismans, S. R., & Beaumont, C. (2003). Symmetric and asymmetric lithopheric extension: Relative effects of frictional-plastic and viscous strain softening. *Journal of Geophysical Research*, *108*(B10), 2496. https://doi.org/10.1029/2002JB002026

Hurich, C. A., Deemer, S. J., Indares, A., & Salisbury, M. (2001). Compositional and metamorphic controls on velocity and reflectivity in the continental crust: An example from the Grenville Province of eastern Québec. *Journal of Geophysical Research*, *106*(B1), 665–682. https://doi.org/10.1029/2000JB900244

Kinck, J. J., Husebye, E. S., & Larsson, F. R. (1993). The Moho depth distribution in Fennoscandia and the regional tectonic evolution from Archean to Permian times. *Precambrian Research*, *64*(1–4), 23–51. https://doi.org/10.1016/0301-9268(93)90067-C

Klausen, M. B., & Larsen, H. C. (2002). East Greenland coast-parallel dike swarm and its role in continental breakup. In M. A. Menzies, S. L. Klemperer, C. J. Ebinger, & J. Baker (Eds.), *Volcanic rifted margins*, *Geological Society of America Special Paper* (pp. 133–158). Boulder, CO: Geological Society of America.

Klingelhöfer, F., Edwards, R. A., Hobbs, R. W., & England, R. W. (2005). Crustal structure of the NE Rockall Trough from wide-angle seismic data modeling. *Journal of Geophysical Research*, *110*, B11105. https://doi.org/10.1029/2005JB003763

Kodaira, S., Goldschmidt-Rokita, A., Hartmann, J. M., Hirschleber, H. B., Iwasaki, T., Kanazawa, T., … Shimamura, H. (1995). Crustal structure of the Lofoten continental margin, off northern Norway, from ocean-bottom seismographic studies. *Geophysical Journal International*, *121*(3), 907–924. https://doi.org/10.1111/j.1365-246X.1995.tb06447.x

Koptev, A., Calais, E., Burov, E., Leroy, S., & Gerya, T. (2015). Dual continental rift systems generated by plume–lithosphere interaction. *Nature Geoscience*, *8*(5), 388–392. https://doi.org/10.1038/ngeo2401

Korenaga, J., Kelemen, P. B., & Holbrook, W. S. (2002). Methods for resolving the origin of large igneous provinces from crustal seismology. *Journal of Geophysical Research*, *107*(B9), 2178. https://doi.org/10.1029/2001JB001030

Kusznir, N. J., & Park, J. K. (1987). The extensional strength of the continental lithosphere: Its dependence on geothermal gradient, and crustal composition and thickness. In M. P. Coward, J. F. Dewey, & P. L. Hancock (Eds.), *Continental extensional tectonics*, *Geological Society Special Publication* (Vol. 28, pp. 35–52). London: The Geological Society.

Kusznir, N. J., Roberts, A., & Bellingham, P. (2015). Deep seismic reflectivity at volcanic margins: Reflections from the petrological Moho or from within the mantle? Paper presented at EGU General Assembly, Vienna.

Kvarven, T., Ebbing, J., Mjelde, R., Faleide, J. I., Libak, A., Thybo, H., … Murai, Y. (2014). Crustal structure across the Møre Margin, mid-Norway, from wide-angle seismic and gravity data. *Tectonophysics*, *626*, 21–40. https://doi.org/10.1016/j.tecto.2014.03.021

Kvarven, T., Mjelde, R., Hjelstuen, B. O., Faleide, J. I., Thybo, H., Flueh, E. R., & Murai, Y. (2016). Crustal composition of the Møre Margin and compilation of a conjugate Atlantic margin transect. *Tectonophysics*, *666*, 144–157. https://doi.org/10.1016/j.tecto.2015.11.002

Larsen, L. M., Pedersen, A. K., Tegner, C., & Duncan, R. A. (2014). Eocene to Miocene igneous activity in NE Greenland: Northward younging of magmatism along the EAst Greenland Margin. *Journal of the Geological Society*, *171*(4), 539–553. https://doi.org/10.1144/jgs2013-118

Lavecchia, A., Thieulot, C., Beekman, F., Cloetingh, S., & Clark, S. (2017). Lithosphere erosion and continental breakup: Interaction of extension, plume upwelling and melting. *Earth and Planetary Science Letters*, *467*, 89–98. https://doi.org/10.1016/j.epsl.2017.03.028

Lavier, L. L., & Manatschal, G. (2006). A mechanism to thin the continental lithosphere at magma-poor margins. *Nature*, *440*, 607–610.

Lien, T. (2005). From rifting to drifting: Effects on the development of deep-water hydrocarbon reservoirs in a passive margin setting, Norwegian sea, *Norsk Geologisk Tidsskrift volume 85 2005 number 4 side 319-332*.

Lister, J. R., & Kerr, R. C. (1991). Fluid-mechanical models of crack propagation and their application to magma transport in dykes. *Journal of Geophysical Research*, *96*, 10,049–10,077.

Lundin, E. R., & Doré, A. G. (1997). A tectonic model for the Norwegian passive margin with implications for the NE Atlantic: Early Cretaceous to break-up. *Journal of the Geological Society*, *154*(3), 545–550. https://doi.org/10.1144/gsjgs.154.3.0545

Lundin, E. R., & Doré, A. G. (2005). NE Atlantic break-up: A re-examination of the Iceland mantle plume model and the Atlantic–Arctic linkage. *Geological Society, London, Petroleum Geology Conference Series*, *6*, 739–754. https://doi.org/10.1144/0060739

Lundin, E. R., & Doré, A. G. (2011). Hyperextension, serpentinization, and weakening: A new paradigm for rifted margin compressional deformation. *Geology*, *39*(4), 347–350. https://doi.org/10.1130/g31499.1

Mandler, H. A. F., & Jokat, W. (1998). The crustal structure of central East Greenland: Results from combined land–sea seismic refraction experiments. *Geophysical Journal International*, *135*(1), 63–76. https://doi.org/10.1046/j.1365-246X.1998.00586.x

Maus, S., Barckhausen, U., Berkenbosch, H., Bournas, N., Brozena, J., Childers, V., … Caratori Tontini, F. (2009). EMAG2: A 2-arc min resolution Earth Magnetic Anomaly Grid compiled from satellite, airborne, and marine magnetic measurements. *Geochemistry, Geophysics, Geosystems*, *10*, Q08005. https://doi.org/10.1029/2009GC002471

Menzies, M. A., Klemperer, S. L., Ebinger, C. J., & Baker, J. (2002). Characteristics of volcanic rifted margins. In M. A. Menzies, et al. (Eds.), *Volcanic rifted margins* (Vol. 362, pp. 1–14). Boulder, CO: Geological Society of America.

Meyer, R., Hertogen, J., Pedersen, R. B., Viereck-Götte, L., & Abratis, M. (2009). Interaction of mantle derived melts with crust during the emplacement of the Vøring Plateau, N.E. Atlantic. *Marine Geology*, *261*(1–4), 3–16. https://doi.org/10.1016/j.margeo.2009.02.007

Meyer, R., van Wijk, J., & Gernigon, L. (2007). The North Atlantic Igneous Province: A review of models for its formation. *Geological Society of America Special Papers*, *430*, 525–552. https://doi.org/10.1130/2007.2430(26)

Mitchell, N. C. (2001). Random sequences of lithologies exposed on the Mid-Atlantic Ridge. *Journal of Geophysical Research*, *106*(B11), 26,365–26,378. https://doi.org/10.1029/2001JB000241

Mjelde, R., Faleide, J. I., Breivik, A. J., & Raum, T. (2009). Lower crustal composition and crustal lineaments on the Vøring Margin, NE Atlantic: A review. *Tectonophysics*, *472*(1–4), 183–193. https://doi.org/10.1016/j.tecto.2008.04.018

Mjelde, R., Goncharov, A., & Müller, R. D. (2013). The Moho: Boundary above upper mantle peridotites or lower crustal eclogites? A global review and new interpretations for passive margins. *Tectonophysics*, *609*, 636–650. https://doi.org/10.1016/j.tecto.2012.03.001

Mjelde, R., Kasahara, J., Shimamura, H., Kamimura, A., Kanazawa, T., Kodaira, S., … Shiobara, H. (2002). Lower crustal seismic velocity-anomalies; magmatic underplating or serpentinized peridotite? Evidence from the Vøring Margin, NE Atlantic. *Marine Geophysical Researches*, *23*(2), 169–183. https://doi.org/10.1023/a:1022480304527

Mjelde, R., Kodaira, S., Hassan, R. K., Goldschmidt-Rokita, A., Tomita, N., Sellevoll, M. A., … Kanazawa, T. (1996). The continent/ocean transition of the Lofoten volcanic margin, N. Norway. *Journal of Geodynamics*, *22*(3–4), 189–206. https://doi.org/10.1016/0264-3707(96)00016-6

Mjelde, R., Kodaira, S., Shimamura, H., Kanazawa, T., Shiobara, H., Berg, E. W., & Riise, O. (1997). Crustal structure of the central part of the Vøring Basin, mid-Norway margin, from ocean bottom seismographs. *Tectonophysics*, *277*(4), 235–257. https://doi.org/10.1016/S0040-1951(97)00028-0

Mjelde, R., Kvarven, T., Faleide, J. I., & Thybo, H. (2016). Lower crustal high-velocity bodies along North Atlantic passive margins, and their link to Caledonian suture zone eclogites and Early Cenozoic magmatism. *Tectonophysics*, *670*, 16–29. https://doi.org/10.1016/j.tecto.2015.11.021

Mjelde, R., Raum, T., Breivik, A., Shimamura, H., Murai, Y., Takanami, T., & Faleide, J. I. (2005). Crustal structure of the Vøring Margin, NE Atlantic: A review of geological implications based on recent OBS data. *Geological Society, London, Petroleum Geology Conference Series*, *6*, 803–813. https://doi.org/10.1144/0060803

Mjelde, R., Raum, T., Digranes, P., Shimamura, H., Shiobara, H., & Kodaira, S. (2003). V_P/V_S ratio along the Vøring Margin, NE Atlantic, derived from OBS data: Implications on lithology and stress field. *Tectonophysics*, *369*(3–4), 175–197. https://doi.org/10.1016/S0040-1951(03)00198-7

Mjelde, R., Raum, T., Kandilarov, A., Murai, Y., & Takanami, T. (2009). Crustal structure and evolution of the outer Møre Margin, NE Atlantic. *Tectonophysics*, *468*(1–4), 224–243. https://doi.org/10.1016/j.tecto.2008.06.003

Mjelde, R., Raum, T., Murai, Y., & Takanami, T. (2007). Continent–ocean-transitions: Review, and a new tectono-magmatic model of the Vøring Plateau, NE Atlantic. *Journal of Geodynamics*, *43*(3), 374–392.

Mjelde, R., Raum, T., Myhren, B., Shimamura, H., Murai, Y., Takanami, T., … Næss, U. (2005). Continent–ocean transition on the Vøring Plateau, NE Atlantic, derived from densely sampled ocean bottom seismometer data. *Journal of Geophysical Research*, *110*, B05101. https://doi.org/10.1029/2004JB003026

Mjelde, R., Shimamura, H., Kanazawa, T., Kodaira, S., Raum, T., & Shiobara, H. (2003). Crustal lineaments, distribution of lower crustal intrusives and structural evolution of the Vøring Margin, NE Atlantic; new insight from wide-angle seismic models. *Tectonophysics*, *369*(3–4), 199–218. https://doi.org/10.1016/S0040-1951(03)00199-9

Mutter, J. C., Talwani, M., & Stoffa, P. L. (1982). Origin of seaward-dipping reflectors in oceanic crust off the Norwegian margin by "subaerial sea-floor spreading". *Geology*, *10*, 353–357.

Neumann, E.-R., Svensen, H., Tegner, C., Planke, S., Thirlwall, M., & Jarvis, K. E. (2013). Sill and lava geochemistry of the mid-Norway and NE Greenland conjugate margins. *Geochemistry, Geophysics, Geosystems*, *14*, 3666–3690. https://doi.org/10.1002/ggge.20224

Nirrengarten, M., Gernigon, L., & Manatschal, G. (2014). Lower crustal bodies in the Møre volcanic rifted margin: Geophysical determination and geological implications. *Tectonophysics*, *636*, 143–157. https://doi.org/10.1016/j.tecto.2014.08.004

Olafsson, I., Sundvor, E., Eldholm, O., & Grue, K. (1992). Møre Margin: Crustal structure from analysis of expanded spread profiles. *Marine Geophysical Researches*, *14*(2), 137–162. https://doi.org/10.1007/bf01204284

O'Reilly, B. M., Hauser, F., Jacob, A. W. B., & Shannon, P. M. (1996). The lithosphere below the Rockall Trough: Wide-angle seismic evidence for extensive serpentinisation. *Tectonophysics*, *255*(1–2), 1–23. https://doi.org/10.1016/0040-1951(95)00149-2

Osmundsen, P. T., & Ebbing, J. (2008). Style of extension offshore mid-Norway and implications for mechanisms of crustal thinning at passive margins. *Tectonics*, *27*, TC6016. https://doi.org/10.1029/2007TC002242

Pérez-Gussinyé, M. (2012). A tectonic model for hyperextension at magma-poor rifted margins: An example from the West Iberia–Newfoundland conjugate margins. *Geological Society, London, Special Publications*, *369*. https://doi.org/10.1144/sp369.19

Peron-Pinvidic, G., & Osmundsen, P. T. (2016). Architecture of the distal and outer domains of the Mid-Norwegian rifted margin: Insights from the Rån–Gjallar ridges system. *Marine and Petroleum Geology*, *77*, 280–299. https://doi.org/10.1016/j.marpetgeo.2016.06.014

Petersen, K. D., & Schiffer, C. (2016). Wilson cycle passive margins: Control of orogenic inheritance on continental breakup. *Gondwana Research*, *39*, 131–144. https://doi.org/10.1016/j.gr.2016.06.012

Planke, S., Millett, J. M., Maharjan, D., Jerram, D. A., Abdelmalak, M. M., Groth, A., … Myklebust, R. (2017). Igneous seismic geomorphology of buried lava fields and coastal escarpments on the Vøring volcanic rifted margin. *Interpretation*, *5*(3), SK161–SK177. https://doi.org/10.1190/int-2016-0164.1

Planke, S., Rasmussen, T., Rey, T., & Myklebust, R. (2005). Seismic characteristics and distribution of volcanic intrusions and hydrothermal vent complexes in the Vøring and Møre basins. In A. G. Doré & B. A. Vining (Eds.), *Petroleum geology: North-west Europe and global perspectives—Proceedings of the 6th Petroleum Geology Conference* (pp. 833–844). London: Geological Society.

Planke, S., Skogseid, J., & Eldholm, O. (1991). Crustal structure off Norway, 62° to 70° north. *Tectonophysics*, *189*(1–4), 91–107. https://doi.org/10.1016/0040-1951(91)90489-F

Planke, S., Svensen, H., Myklebust, R., Bannister, S., Manton, B., & Lorenz, L. (2015). *Geophysics and remote sensing* (pp. 1-16). Springer Berlin. https://doi.org/10.1007/11157_2014_6

Planke, S., Symonds, P. A., Avelstad, E., & Skogseid, J. (2000). Seismic volcanostratigraphy of large-volume basaltic extrusive complexes on rifted margins. *Journal of Geophysical Research*, *105*, 19,333–19,351.

Raum, T., Mjelde, R., Digranes, P., Shimamura, H., Shiobara, H., Kodaira, S., … Thorbjørnsen, T. (2002). Crustal structure of the southern part of the Vøring Basin, mid-Norway margin, from wide-angle seismic and gravity data. *Tectonophysics*, *355*(1–4), 99–126. https://doi.org/10.1016/S0040-1951(02)00136-1

Raum, T., Mjelde, R., Shimamura, H., Murai, Y., Bråstein, E., Karpuz, R. M., … Kolstø, H. J. (2006). Crustal structure and evolution of the southern Vøring Basin and Vøring Transform Margin, NE Atlantic. *Tectonophysics*, *415*(1–4), 167–202. https://doi.org/10.1016/j.tecto.2005.12.008

Ren, S., Faleide, J. I., Eldholm, O., Skogseid, J., & Gradstein, F. (2003). Late Cretaceous–Paleocene tectonic development of the NW Vøring Basin. *Marine and Petroleum Geology*, *20*(2), 177–206. https://doi.org/10.1016/S0264-8172(03)00005-9

Ren, S., Skogseid, J., & Eldholm, O. (1998). Late Cretaceous–Paleocene extension on the Vøring volcanic margin. *Marine Geophysical Researches*, *20*(4), 343–369. https://doi.org/10.1023/a:1004554217069

Reston, T. J. (2007). Extension discrepancy at North Atlantic nonvolcanic rifted margins: Depth-dependent stretching or unrecognized faulting? *Geology*, *35*(04), 367–370.

Reynisson, R. F., Ebbing, J., Lundin, E., & Osmundsen, P. T. (2010). Properties and distribution of lower crustal bodies on the mid-Norwegian margin. *Geological Society, London, Petroleum Geology Conference Series*, *7*, 843–854. https://doi.org/10.1144/0070843

Reynolds, P., Planke, S., Millett, J. M., Jerram, D. A., Trulsvik, M., Schofield, N., & Myklebust, R. (2017). Hydrothermal vent complexes offshore northeast Greenland: A potential role in driving the PETM. *Earth and Planetary Science Letters*, *467*, 72–78. https://doi.org/10.1016/j.epsl.2017.03.031

Roberts, A. W., White, R. S., & Christie, P. A. F. (2009). Imaging igneous rocks on the North Atlantic rifted continental margin. *Geophysical Journal International*, *179*(2), 1024–1038. https://doi.org/10.1111/j.1365-246X.2009.04306.x

Rosenbaum, G., Weinberg, R. F., & Regenauer-Lieb, K. (2008). The geodynamics of lithospheric extension. *Tectonophysics*, *458*(1-4), 1–8.

Rouzo, S., Klingelhöfer, F., Jonquet-Kolstø, H., Karpuz, R., Kravik, K., Mjelde, R., … Géli, L. (2006). 2-D and 3-D modelling of wide-angle seismic data: An example from the Vøring volcanic passive margin. *Marine Geophysical Researches*, *27*(3), 181–199. https://doi.org/10.1007/s11001-006-0001-3

Rubin, A. M. (1995). Propagation of magma-filled cracks. *Annual Review of Earth and Planetary Sciences*, *23*(1), 287–336. https://doi.org/10.1146/annurev.ea.23.050195.001443

Saltus, R. W., & Blakely, R. J. (2011). Unique geologic insights from "non-unique" gravity and magnetic interpretation. *GSA Today*, *21*, 4–10.

Sandwell, D. T., & Smith, W. H. F. (2009). Global marine gravity from retracked Geosat and ERS-1 altimetry: Ridge segmentation versus spreading rate. *Journal of Geophysical Research*, *114*, B01411. https://doi.org/10.1029/2008JB006008

Saunders, A. D., Fitton, J. G., Kerr, A. C., Norry, M. J., & Kent, R. W. (1997). The North Atlantic igneous province. In J. J. Mahoney & M. F. Coffin (Eds.), *Large igneous provinces: Continental, oceanic, and planetary flood volcanism* (pp. 45–93). Washington, DC: American Geophysical Union.

Scheck-Wenderoth, M., Raum, T., Faleide, J. I., Mjelde, R., & Horsfield, B. (2007). The transition from the continent to the ocean: A deeper view on the Norwegian margin. *Journal of the Geological Society*, *164*(4), 855–868. https://doi.org/10.1144/0016-76492006-131

Schiffer, C., Balling, N., Ebbing, J., Jacobsen, B. H., & Nielsen, S. B. (2016). Geophysical-petrological modelling of the East Greenland Caledonides—Isostatic support from crust and upper mantle. *Tectonophysics*, *692*(Part A), 44–57. https://doi.org/10.1016/j.tecto.2016.06.023

Schiffer, C., Jacobsen, B. H., Balling, N., Ebbing, J., & Nielsen, S. B. (2015). The East Greenland Caledonides—Teleseismic signature, gravity and isostasy. *Geophysical Journal International*, *203*(2), 1400–1418. https://doi.org/10.1093/gji/ggv373

Schlindwein, V., & Jokat, W. (1999). Structure and evolution of the continental crust of northern East Greenland from integrated geophysical studies. *Journal of Geophysical Research*, *104*, 15,227–15,245.

Schlindwein, V., & Jokat, W. (2000). Post-collisional extension of the East Greenland Caledonides: A geophysical perspective. *Geophysical Journal International*, *140*(3), 559–567. https://doi.org/10.1046/j.1365-246X.2000.00036.x

Schmidt-Aursch, M. C., & Jokat, W. (2005). The crustal structure of central East Greenland—I: From the Caledonian orogen to the Tertiary igneous province. *Geophysical Journal International*, *160*(2), 736–752. https://doi.org/10.1111/j.1365-246X.2005.02514.x

Skelton, A., Whitmarsh, R., Arghe, F., Crill, P., & Koyi, H. (2005). Constraining the rate and extent of mantle serpentinization from seismic and petrological data: Implications for chemosynthesis and tectonic processes. *Geofluids*, *5*(3), 153–164. https://doi.org/10.1111/j.1468-8123.2005.00111.x

Skogseid, J. (2001). Volcanic margins: Geodynamic and exploration aspects. *Marine and Petroleum Geology*, *18*, 457–461.

Skogseid, J., & Eldholm, O. (1989). Vøring Plateau continental margin: Seismic interpretation, stratigraphy, and vertical movements. In O. Eldholm, et al. (Eds.), *Proceedings of the ODP, Scientific Results*, *104*, (pp. 993–1030). College Station, TX: Ocean Drilling Program.

Skogseid, J., Planke, S., Faleide, J. I., Pedersen, T., Eldholm, O., & Neverdal, F. (2000). NE Atlantic continental rifting and volcanic margin formation. In A. E. A. Nottvedt (Ed.), *Dynamics of the Norwegian margin* (pp. 295–326). London: Geological Society, London, Special Publications.

Stratford, W., Thybo, H., Faleide, J. I., Olesen, O., & Tryggvason, A. (2009). New Moho map for onshore southern Norway. *Geophysical Journal International*, *178*(3), 1755–1765. https://doi.org/10.1111/j.1365-246X.2009.04240.x

Svensen, H., Planke, S., Malthe-Sorenssen, A., Jamtveit, B., Myklebust, R., Rasmussen Eidem, T., & Rey, S. S. (2004). Release of methane from a volcanic basin as a mechanism for initial Eocene global warming. *Nature*, *429*(6991), 542–545.

Tegner, C., Lesher, C. E., Larsen, L. M., & Watt, W. S. (1998). Evidence from the rare-earth-element record of mantle melting for cooling of the Tertiary Iceland plume. *Nature*, *395*(6702), 591–594. http://www.nature.com/nature/journal/v395/n6702/suppinfo/395591a0_S1.html

Theissen-Krah, S., Zastrozhnov, D., Abdelmalak, M. M., Schmid, D. W., Faleide, J. I., & Gernigon, L. (2017). Tectonic evolution and extension at the Møre Margin—Offshore mid-Norway. *Tectonophysics*, *721*, 227–238.

Thomsen, L. (1986). Weak elastic anisotropy. *Geophysics*, *51*(10), 1954–1966. https://doi.org/10.1190/1.1442051

Tsikalas, F., Faleide, J. I., Eldholm, O., & Antonio Blaich, O. (2012). 5 - The NE Atlantic conjugate margins. In D. G. R. W. Bally (Ed.), *Regional geology and tectonics: Phanerozoic passive margins, cratonic basins and global tectonic maps* (pp. 140–201). Boston, MA: Elsevier. https://doi.org/10.1016/B978-0-444-56357-6.00004-4

Tsikalas, F., Faleide, J. I., & Kuznir, N. J. (2008). Along-strike variations in rifted margin crustal architecture and lithosphere thinning between northern Vøring and Lofoten margin segments off mid-Norway. *Tectonophysics*, *458*, 68–81.

Verhoef, J., MacNab, R., Roest, W., Arkani-Hamed, J., & Members of the Project Team (1996). Magnetic anomalies of the Arctic and North Atlantic Oceans and adjacent land areas (GAMM-AA5: Gridded Aeromagnetic and Marine Magnetics of the North Atlantic and Arctic, 5km) *Rep. 3125*, Geological Survey of Canada, Open File Report 3125a.

Voss, M., & Jokat, W. (2007). Continent–ocean transition and voluminous magmatic underplating derived from *P*-wave velocity modelling of the East Greenland continental margin. *Geophysical Journal International*, *170*(580-604).

Voss, M., Schmidt-Aursch, M. C., & Wilfried, J. (2009). Variations in magmatic processes along the East Greenland volcanic margin. *Geophysical Journal International*, *177*, 755–782.

Wangen, M., Mjelde, R., & Faleide, J. I. (2011). The extension of the Vøring Margin (NE Atlantic) in case of different degrees of magmatic underplating. *Basin Research*, *23*(1), 83–100. https://doi.org/10.1111/j.1365-2117.2010.00467.x

Weigel, W., Flüh, E. R., Miller, H., Butzke, A., Dehghani, G. A., Gebhardt, V., … Groekort Study Group (1995). Investigations of the East Greenland continental margin between 70° and 72°N by deep seismic sounding and gravity studies. *Marine Geophysical Researches*, *17*(2), 167–199. https://doi.org/10.1007/bf01203425

White, R. S. (1988). A hot-spot model for early Tertiary volcanism on the N Atlantic. In A. C. Morton & L. M. Parson (Eds.), *Early Tertiary volcanism and the opening of the NE Atlantic*, *Geological Soceity Special Publication* (pp. 3–13).

White, R. S., McKenzie, D., & O'Nions, R. K. (1992). Oceanic crustal thickness from seismic measurements and rare earth element inversions. *Journal of Geophysical Research*, *97*(B13), 19,683–19,715. https://doi.org/10.1029/92JB01749

White, R. S., & McKenzie, D. P. (1989). Magmatism at rift zones: The generation of volcanic continental margins and flood basalts. *Journal of Geophysical Research*, *94*, 7685–7729.

White, R. S., & Smith, L. K. (2009). Crustal structure of the Hatton and the conjugate East Greenland rifted volcanic margins, NE Atlantic. *Journal of Geophysical Research*, *114*, B02305. https://doi.org/10.1029/2008JB005856

White, R. S., Smith, L. K., Roberts, A. W., Christie, P. A. F., Kusznir, N. J., & the rest of the iSIMM Team (2008). Lower-crustal intrusion on the North Atlantic continental margin. *Nature*, *452*, 460–465.

White, R. S., Spence, G. D., Fowler, S. R., McKenzie, D. P., Westbrook, G. K., & Bowen, A. N. (1987). Magmatism at rifted continental margins. *Nature*, *330*, 439–444.

White, W. M., & Klein, E. M. (2014). Composition of the oceanic crust. In *Treatise on geochemistry* (2nd ed., pp. 457-496). Amsterdam, Netherlands: Elsevier.

Wilson, M., & Wheeler, W. (2002). Magma migration through the continental crust: 3-D seismic and thermo-mechanical constraints on sites of crustal contamination. In *Eos Transactions, American Geophysical Union* (pp. F1407). Washington, DC.

Zehnder, M. C., Mutter, J., & Buhl, P. (1990). Deep seismic and geochemical constraints on the nature of rift-induced magmatism during breakup of the North Atlantic, Siesmic probing of continents and their margins. *Tectonophysics*, *173*(1), 545-565. https://doi.org/10.1016/0040-1951(90)90245-4

Ziegler, P. A. (1988). *Evolution of the Arctic–North Atlantic and the Western Tethys* (Vol. 43). American Association of Petroleum Geologist Memoir.

Ziegler, P. A., & Cloetingh, S. (2004). Dynamic processes controlling evolution of rifted basins. *Earth Science Reviews*, *64*, 1–50.